Lund University GEM thesis series nr 28

Evaluation of methodology for estimating crop yield from multispectral UAV images

A case study at SITES Lönnstorp, Sweden

Ashish Vivekar

2019

Department of Physical Geography and Ecosystem Science

Lund University

Sölvegatan 12

S-223 62 Lund

Sweden

LUND UNIVERSITY

UNIVERSITY OF TWENTE.

ITC FACULTY OF GEO-INFORMATION SCIENCE AND EARTH OBSERVATION

Evaluation of methodology for estimating crop yield from multispectral UAV images

A case study at SITES Lönnstorp, Sweden

Ashish Vivekar

Thesis submitted to the department of Physical Geography and Ecosystem Science, Lund University, in partial fulfilment of the requirements for the degree of Master of Science in Geo-information Science and Earth Observation for Environmental Modelling and Management

Thesis assessment Board

Supervisor: *Dr., Lars Eklundh* (Lund University)

Exam committee:

Examiner 1: Dr. Jonas Ardö

Examiner 2: Dr. Feng Tian

Disclaimer

This document describes work undertaken as part of a program of study at the University of Lund. All views and opinions expressed therein remain the sole responsibility of the author, and do not necessarily represent those of the institute.

Course title: Geo-information Science and Earth Observation for Environmental Modelling and Management (GEM)

Level: Master of Science (MSc)

Course duration: January 20*19* until June 20*19*

Consortium partners:

The GEM master program is a cooperation of departments at 5 different universities:

University of Twente, ITC (The Netherlands)

University of Lund (Sweden)

University of Southampton (UK)

University of Warsaw (Poland)

University of Iceland (Iceland)

Abstract

Adaptation of modern Unmanned Aerial Vehicle (UAV) and multispectral sensor technology in agriculture can enhance the capacity to accurately monitor crops. But this technology comes with its own set of challenges. The major challenge is the understanding of radiometric distortions, which is particularly important while comparing data over different lighting conditions. The study developed and assessed a methodology for extracting radiometrically corrected reflectance values for multi-temporal datasets. The empirical line method is used to calibrate the images using spectrally stable panels. The methodology is assessed by studying the association between three vegetation indices namely Normalized Difference Vegetation Index (NDVI), Soil Adjusted Vegetation Index (SAVI) and Difference Vegetation Index (DVI) with corresponding crop yield, crop height and fixed tower sensor data. The radiometric correction techniques delivered reasonably satisfactory results which was revealed by very strong Pearson correlation (r = 0.87 - 0.95) between fixed tower and UAV sensors. The investigation also identified that the vegetation indices dependency varied positively with (fresh) yield of legume ley, from moderate to high, on the first harvest date (11th May 2019) as well as on the second harvest date (26th July 2019). The Pearson correlation (r) and Spearman rank correlation coefficients (r_s) ranged between 0.55 and 0.89 on the first harvest date and between 0.49 and 0.79 on the second harvest. Comparable results were obtained for other crops but only at certain stages of crop development. The analysis revealed moderate to high positive relationship (r = 0.45 – 0.87) between vegetation indices (NDVI and SAVI) and crop height except on 21st August 2019 dataset, where the relationship was rather weak (r = 0.19 and 0.04). DVI showed similar trend (r = 0.62 – 0.81), except in the case of 26th July 2019 and 21st August 2019 datasets, where correlation coefficients were r = 0.19 and r = -0.02 respectively. It was also observed that 6 datasets over the growing period are not enough to clearly see the complete crop phenology, although the comparison of NDVI, SAVI and DVI indicated similar patterns. The inability in reflecting the complete phenology of various crops was mainly due to less frequent data acquisition at development stages. Nonetheless, very high positive correlation between vegetation indices from UAV sensor and fixed tower sensor validated the capability of UAV sensor to monitor the crops over various stages.

Acknowledgements

I extend my deep sense of gratitude and sincere thanks to my research supervisor Dr. Lars Eklundh for the encouragement, assistance, guidance and patience during the course of my research and thesis. I also offer my sincere appreciation for the learning opportunities provided by you.

I offer special thanks to Dr. Per-Ola Olsson and Dr. Virginia Garcia for helping with technical and theoretical difficulties, valuable suggestions and generous guidance. Without your support it would have been difficult to finish this research work.

I thank Dr. Johannes Albertsson for providing invaluable information and insights about the study area. I deeply appreciate your prompt replies to my queries. I thank Ryan Davidson for helping me with UAV flights and data. I also thank the staff of SLU for their support over various stages of the project.

I thank Ricardo Guillén and Rafael Przybyszewski for helping out with IT issues. Your prompt help saved us a lot of time.

In addition, I would like to thank all my colleagues, faculties and other staffs from ITC and Lund University for making this experience worth remembering. I would like to acknowledge my colleagues Aiman Shahpurwala, Femke Pijcke, Lone Mokkenstorm, Maria Jäppinen, Mathias Welp, Mihai Patrascu, and Shangharsha Thapa for constructive comments, healthy discussions, corrections and moral support.

I thank Naval Agrawal and Shurakshya Dhakal for checking grammar and providing invaluable comments to improve quality of writing.

Finally, I would like to thank all my friends, well-wishers and individuals who directly or indirectly helped me finish this research project.

Contents

List of Figures

List of Tables

List of Acronyms

AI - Agroecological intensification
AVHRR- Advanced Very High Resolution Radiometer
BBA - Bundle Block Adjustment
BRDF - Bidirectional Reflectance Distribution Function
CSM - Crop Surface Model
DEM - Digital Elevation Model
DSM - Digital Surface Model
DTM - Digital Terrain Model
DVI - Difference Vegetation Index
EXIF - Exchangeable Image File Format
FAO - Food and Agriculture Organization
FPS - Frames per Second
GCP - Ground Control Point
GPS - Global Positioning Systems
IMU - Inertial Measurement Unit
ISO - International Organization of Standardization
LAI - Leaf Area Index
MODIS- Moderate Resolution Imaging Spectroradiometer
NDVI - Normalized Difference Vegetation Index
NIR - Near Infrared
ORG - Organic
PA - Precision Agriculture
PER - Perennial
REF - Reference
RTK - Real Time Kinematics
SAFE - SITES Agroecological Field Experiment
SAVI - Soil Adjusted Vegetation Index
SDG - Sustainable Development Goal
SfM - Structure from Motion
SHMI - Sveriges Meteorologiska och Hydrologiska Institut
SITES - Swedish Infrastructure for Ecosystem Science
SLU - Swedish- Sveriges Lantbruks Universitet, English- Swedish University of Agricultural Sciences
UAS - Unmanned Aerial System
UAV - Unmanned Aerial Vehicle
UN - United Nations
VHR - Very High Resolution
VI - Vegetation Index

1. Introduction

A rapid increase in food demand has increased pressure on the agriculture sector, which in turn is further affected by the climate change. United Nations (UN) sustainable development goal (SDG) #2 advocates sustainable agriculture to achieve food security and improved nutrition. The Food and Agriculture Organization of the United Nations (FAO) states the requirement to double global food production by 2050 to meet the demand of rapidly increasing population which population which must be attained against the backdrop of climate change and shortfall of resources (FAO, 2009). It is estimated that 90% of increase in global crop production (80% in developing countries) is expected to come from higher yields and increased cropping intensity till 2050 (FAO, 2009). To accommodate these changes, we need to find an effective way to monitor the crop growth and yields. Furthermore, monitoring crop growth and crop production is highly crucial in understanding productivity (Singh, n.d.) (Fan et al., 2011). Growth and yield of the crops are affected by many factors including genetic potential, soil types, management practices, biotic stressors (pests, fungi, bacteria, weeds etc.,) and abiotic stressors (drought, salinity, low or high temperatures etc.,) (Dadhwal, 2004). To understand the impact of these factors, especially the stressors, there is a need to develop techniques that assesses the structure and function of plants during various growth stages. This can provide valuable information on required measures to be taken for increasing crop yield and productivity. Effective early intervention can help improve crop health, production efficiency and reduce losses. Various types of RS (Remote-Sensing) sensors and platforms are applicable for this purpose.

Observations from the Unmanned Aerial Vehicles (UAV) remote sensing can help detect various soil characteristics and identify plants under stressful conditions that can affect crop yield and productivity. UAV-based crop yield estimation could help individual farmers to monitor and assess the crop growth and identify problems early, avoiding low yields due to lack of timely monitoring (Vega, Ramírez, Saiz, & Rosúa, 2015).

UAV platforms provide birds-eye-view of the area and can carry a wide array of sensors for monitoring and mapping the agricultural land. UAVs are not only limited to agriculture; they have been widely used in forestry, mining, urban planning, and land management. Many organizations have developed UAVs in different shapes and sizes for specific applications. Factors which determine the choice of UAV for remote sensing are: weightlifting capacity, flight stamina, ease of flying, ease of handling, stability in wind, availability of landing space, and the area to be mapped (Hunt, Cavigelli, Daughtry, McMurtrey, & Walthall, 2005). UAVs also known as drones can be divided into two broad categories: Fixed-wing and Rotary-blade. Each category has its advantages and disadvantages.

Fixed wings UAVs, as the name suggests, use rigid wing structure to generate lift and are propelled forward by the thrust from the engine or the propellers. Whereas, Rotary wings UAVs have multiple rotors (usually 4-8) to provide thrust as well as lift. Fixed wing UAVs provide longer range, greater stability, higher endurance, and linear flight but are more expensive than their rotary wing counterparts. Fixed wings UAVs need larger landing area, are less compact and are more challenging to fly. Whereas, rotary wing UAVs are less expensive and provide greater maneuverability and higher payload capacity. Furthermore, rotary wing UAVs are compact and easy to use, but they are less stable in wind and have shorter range (DroneDeploy, 2017). Rotary wing UAVs are better for mapping and monitoring small areas. They have the ability to hover mid-flight and their slower movement allows the user to have the desired image overlap to make high quality maps. Fixed wing UAVs are better for mapping or inspecting pipelines and electricity lines or any other linear areas. UAVs can carry various type of sensors including Red Green Blue (RGB), multispectral, thermal or even Lidar sensors for earth observation and data acquisition (Effiom, 2018).

In recent times, light-weight multispectral sensors enabled UAVs have become more efficient airborne imaging platforms. They offer cost-effective data collection methods with high spatial resolution and desired temporal resolution. Furthermore, such UAVs have a high tolerance against atmospheric disturbances and cloud cover.

Though the UAVs are typically more suitable for small regions, they can also be used to complement regional-level crop estimation for more accurate results. Traditionally, data samples are collected from in situ measurements, surveys, and crop-cutting experiments in many developing countries (Singh, n.d.). The local UAV based crop estimation can enable farmers to plan their farming related finances more effectively. By upscaling estimations, policy makers can plan the distribution of agricultural resources in national and international markets. Policy makers can expediently plan effective policies for import and export of crops and thus effectively assist in developing agricultural economies (GSARS, 2017).

Recent developments in UAV remote sensing technologies provide better image quality in different spectrums and higher processing capabilities, which can be adapted for Precision Agriculture (PA). PA requires ultra-high spatial (appx. 1cm) as well as high temporal resolution imagery. The unavailability of such resolution from satellite imagery, high costs (procurement and operational) associated with it, and often cloud cover make it difficult to accurately provide valuable outputs for PA (Hunt et al., 2005). The high-resolution images and the maps of different crop growth stages obtained from the UAVs are critical in PA to support the cropping management strategy of farmers (Bendig et al., 2015). In addition, accurate information on the developing stage of crop growth requires finer temporal resolution than satellite image. The finer temporal resolution imagery of agricultural

fields from UAV observation can help provide dynamic solutions and quick decision making. Thus, compared to the satellite acquisitions, UAVs, with their capacity to provide finer spatial and temporal resolution data for a study area of the size of farming lands shows cost effectiveness to the data collection process (Vega et al., 2015).

Previous works have established a credible ground for extracting crop parameters using UAV-based sensors (e.g., RGB, thermal, multispectral and hyperspectral sensors) of varying complexity and conceptual settings (Bendig et al., 2015; Candiago, Remondino, De Giglio, Dubbini, & Gattelli, 2015; De Biasio, Fritz, & Leitner, 2013; Di Gennaro et al., 2018; Possoch et al., 2016; Zhou et al., 2017). The process of extracting plant parameters are continuously evolving through the use of spectral data. The vegetation reflectance captured by multispectral sensors are found to be good estimators of crop biomass, yield, canopy percentage, leaf area index (LAI) and chlorophyll content (Daughtry, Walthall, Kim, de Colstoun, & McMurtrey, 2000; Gitelson, 2004). Vegetation indices (VIs) are methods based on processing the measured electromagnetic radiation, used by scientists to assess physical and chemical properties of vegetation. VIs takes advantage of differences in the reflectance of plants at different bandwidths. These are reliable metrics that are effectively used for diagnosing the health condition of plants, and consequently, these metrics provide important information about plants that may be potentially stressed (Pettorelli, 2013).

Past researches have demonstrated the enormous potential of UAV imagery for monitoring and assessing many agricultural and environmental factors (Zhang & Kovacs, 2012). These techniques allow farmers to overcome the shortcomings of conventional methods. For example, traditionally herbicides were applied in a homogenous way over an entire field. However, because there is variations in the distribution of weeds in the field, by employing UAV technology, farmers can benefit from precision agriculture by making patch specific corrective actions (Gómez-Candón, De Castro, & López-Granados, 2014).

Like PA, plant phenotyping relies on extensive studies of various stages of crop cycle. Plant phenotyping is the study related with quantitative measurement of the structural and functional properties of plants. This is especially important in terms of food security in the context of climate change and resource scarcity (Laboratory, 2019). UAVs can provide high temporal resolution time series which can be used for monitoring crop growth, crop health and the effectiveness of the crop management strategy. A study by Yu et al. (2016) investigated the relationship between crop yield of soybean fields with phenology data. The team developed a dual-camera high throughput phenotyping (HTP) platform on a UAV and collected time series of soybean fields. They used random forest supervised classification to determine crop geometry and found high correlation with the yield. The researchers improved the model significantly by introducing plot row length (calculated as the ratio of ‘number of “crop” pixels in the row’ and ‘total number of the three center rows of pixels’ for each plot)

as covariate. From the perspective of image resolution and time of data collection, Vega et al. (2015) tried to establish the relation between normalized difference vegetation index (NDVI) and crop biomass for sunflower crop in southern Spain. They found statistically significant correlation coefficients of linear regressions for NDVI and grain yield, aerial biomass and nitrogen content except during the early phase in the growing season. However, the study did not find any effects from the image resolution (30 x 30 and 100 x 100 cm pixel size) and the time-of-day (i.e., midday and afternoon) of image acquisition on results.

On the other hand, Yue et al. (2017) used a completely different approach for estimating crop yield and growth monitoring. The primary objective was to correctly estimate the AGB (i.e., Above Ground Biomass) from a hyperspectral sensor mounted on UAV. Images from hyperspectral sensor was then used to calculate crop height and reflectance of winter wheat crop and these 2 parameters were compared with band specific VI's. The study emphasized more on accuracy of crop height model for AGB estimation. The result showed incorporating additional parameters such as crop height model significantly improved the accuracy of AGB estimations.

There are few studies done to estimate crop yields from UAV datasets such as Senthilnath, Kandukuri, Dokania, and Ramesh (2017), Hunt et al. (2005), Ziliani, Parkes, Hoteit, and McCabe (2018) and Yemane Tumlisan (2017). However, many of the researchers worked only with RGB sensors. These RGB sensors have limited capability for agricultural applications and the researchers were unable to explain the effect of radiometric variations or they do not focus on it at all. Radiometric accuracy is important while working on phenological data since the images from separate times are exposed to different illumination conditions and can significantly affect the results.

2. Research Aim and Objectives

The aim of this thesis is to quantitatively assess the relationship between crop phenology and three different vegetation indices derived from multispectral UAV imagery. This aim is achieved by developing and applying a novel method to derive radiometrically correct vegetation reflectance from UAV imagery. The relationship between vegetation indices and crop yield will be tested in a Swedish agricultural area, and the temporal pattern of the crops' phenological stages (i.e. sowing, emergence, maturing and harvest will also be analysed using 6 datasets collected over the growing season. The underlying assumption being that 'greener crop will have higher yield'.

It is postulated that radiometrically corrected imagery will provide an accurate estimation of both crop yield and crop phenology, where higher VIs would correspond to higher yield and biomass. The following research questions are formulated to test this hypothesis and reach the objectives:

2.1. What is the accuracy of the method for deriving radiometrically correct images from multispectral UAV imagery?

2.2. What is the relationship between vegetation indices derived from multispectral UAV imagery and crop yield of selected crops in a Swedish agricultural area?

2.3. Which vegetation index (NDVI, SAVI, or DVI) gives best estimation for crop yield?

2.4. How well do NDVI, SAVI, and DVI explain crop phenology stages?

3. Scope of Research and Study Area

The research conducted was exploratory in nature and based on routine data collected from the SITES (Swedish Infrastructure for Ecosystem Science) spectral monitoring program (http://www.fieldsites.se). SITES Spectral Program collects data from their fixed and mobile platform through multispectral sensors and phenology cameras. Apart from recording incoming and reflected solar radiation they also design short-term and long-term crop experiments, which include preparation of soil, sowing, adding manure and fertilizers, irrigation, harvesting, crop rotation and recording all the observations and measurements in a database. SITES extend opportunities for researchers to use the data collected at their stations. Researchers utilizing this facility usually focus on design, sustainable development and assessment of agroecosystems in conventional and ecological farming.

Source: (Swedish University of Agricultural Sciences, 2018)

Figure 1: Location of SITES field research stations.

In this study, data was used from one of the eight SITES Spectral stations namely Lönnstorp situated in Sweden. The central point of the study area is located at longitude 55.6688^0 N and 13.1095^0 E (figure 1). The Lönnstorp site is classified as humid continental climate according to the Köppen climate classification and is classified as Nemoral biome zone according to the Walter classification system. The station was established in 1969 but the area was conventionally farmed until 1993. Later, parts of it were converted into certified organic farming. The infrastructure is mainly used by SLU Swedish University of Agricultural Sciences (Sveriges lantbruksuniversitet) for agricultural research with emphasis on cropping system dynamics. The SITES Lönnstorp station has 60 hectares of conventional farmland and 18 hectares of certified organic farmland.

SITES started a long-term experiment called SITES Agroecological Field Experiment (SAFE) in 2015-2016. SAFE consist of four replicates of the experiments, each of this replicate is called as a block namely SAFE A, B, C and D. Due to time constraints, in this study, data is analyzed only from SAFE A, which consists of one replicate.

The study area lies in the south-west of Skåne, situated 12 kilometers northeast of Malmö (Sweden) at Lönnstorp. The infrastructure jointly belongs to SLU and SITES. The facility consists of 14-hectare SAFE experiment. The area is approximately 14 meters above mean sea level and the soil type is loam consisting of 15% clay and 3 % organic matter. This research station was selected because it is equipped with the necessary infrastructure and it offers facilities to conduct experiment in southern Swedish agroecosystems. The total area of the actual plot is slightly more than 2 hectares.

Figure 2: SAFE A block with 18 plots divided into 4 cropping systems namely Agro-ecological intensification (AI), Organic (ORG), Perennial (PER) and Reference (REF). based on data from SITES.

SLU and SITES collaborated in designing the experiment to incorporate multitude of different cropping patterns with varieties of crops. The objective of utilizing multiple crops with different management strategies was to get more variability and heterogeneity in the available space. The drawback of this method is that it reduces the number of samples of each type. The research evaluates four management strategies namely organic, conventional, agro-ecological intensification (AI) and perennial (figure 2). Eight plots employing AI management system were sowed with Legume ley; four plots employing organic management system were sowed with legume ley, spring wheat/faba bean (intercropping), winter wheat and spring barley/lupine (intercropping), respectively; four plots were designated as the reference system and were sowed with winter wheat, sugar beet, spring

barley and oilseed rape (hairy vetch), respectively; and the last two plots were sowed with perennial wheatgrass Kernza® (*Thinopyrum intermedium*) and Kernza®/Lucerne (alfalfa) intercropping, respectively as shown in figure 3. All the crops, except legume ley, were sown only on a single plot; this restricted the sample size of these crops to just one. Some of the plots in the field were sown and harvested at different dates; furthermore, few of these plots with intercropping had more than one crop. Figure 3 shows the distribution of crops in study area. Additionally, the data using UAV was collected for all the plots at the same time irrespective of the different sowing and harvesting dates. Additionally, we gathered data from only a single season, the summer of 2018, which incidentally turned out to be warmer and drier than average (Liberto, 2018). Although the RGB dataset was available to us, we used only multispectral data because the NIR (i.e., Near Infrared) band is sensitive to vegetation and the derived indices are good indicators of the greenness in the vegetation (Mutanga et al. 2012).

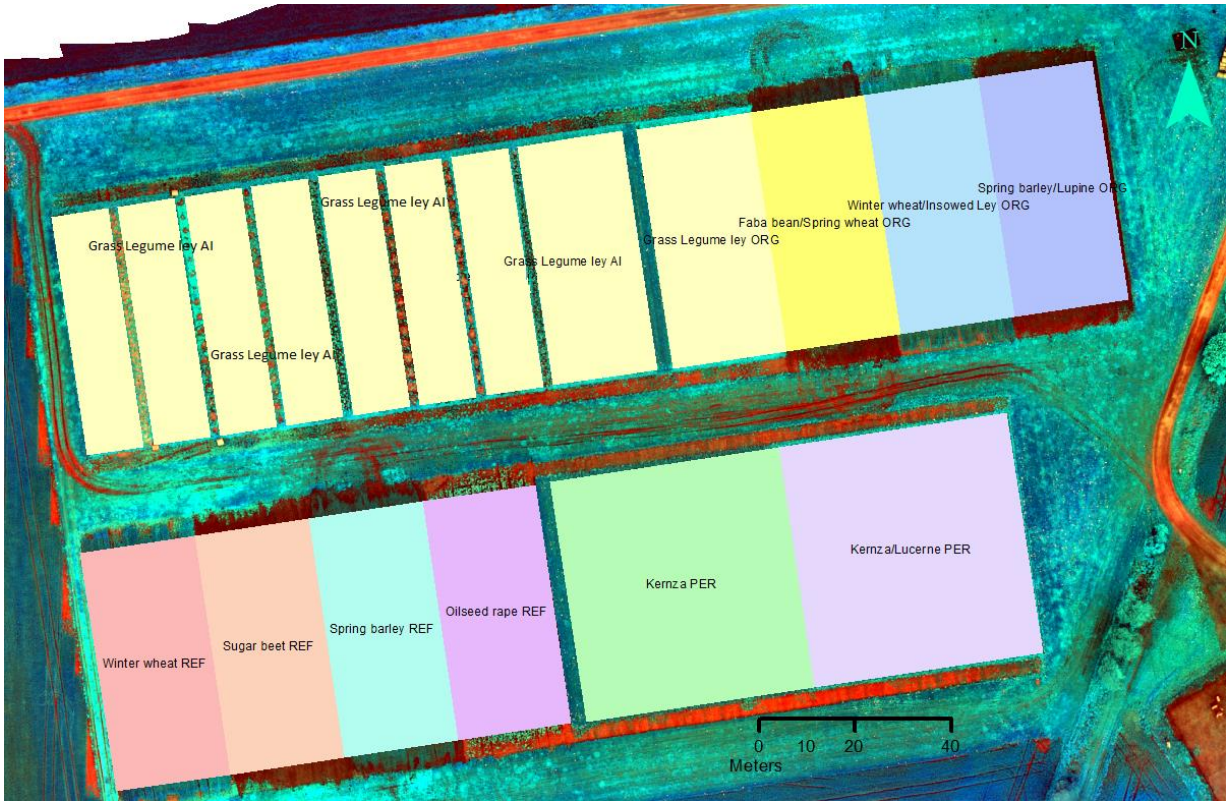

Figure 3: False colour composite (11th May 2018) of study area representing polygons with all the crops and management system in SAFE A.

4. UAV Image Processing Framework

4.1. Geometric Correction

Photogrammetry in remote sensing is defined as the process of extracting reliable spatial measurements of physical entities from captured images. The objective is to derive three-dimensional information from two-dimensional data. Geometric correction is one of the most important steps in Photogrammetry; it helps reduce the error between physical objects present in the image with respect to its location in the real world. Traditionally, geometric correction in UAV remote sensing is based on ground control points (GCPs). GCPs are the point features that are easily and distinctly identifiable in the aerial images and have known geolocations or highly accurate recorded ground coordinates. A GCP determines the relationship between the raw image and the ground by associating the pixel and line image coordinates to the x, y, and z coordinates on the ground (PCI Geomatics, 2018); this process is known as geo-referencing. It is important to have an optimum number of GCPs evenly distributed to increase the accuracy of geo-referencing. With the advent of advance Global Positioning Systems (GPS) and Inertial Measurement Units (IMU) technologies, we can achieve high accuracy of geo-referencing (Petovello, 2003).

Since UAVs capture images at much lower altitudes than satellites, they produce high resolution imagery (Hunt et al., 2005). Even though UVAs based imagery resolution is as high as a centimeter per pixel the downside of lower altitude is reduced ground footprint of the sensors, thus more images are required to generate the orthomosaic (Wijesingha, 2016). In simple words, orthomosaic can be defined as a single scene formed by stitching together geo-rectified tiles of images. To manage the sequencing and orientation of substantial number of images captured, various computer vision techniques are implemented, such as Structure from Motion (SfM). Many organizations have developed software packages capable of performing SfM processes. Some popular open source packages are APERO, MICMAC, VisualSFM and OpenMVG; in addition to the open source packages are commercial software such as Agisoft Metashape and Pix4D (Dall'Asta & Roncella, 2014).

The basic principle underlying these SfM software is that the orientation and sequencing of the images generate an image block that is used to construct a three-dimension structure of the scene. To enable this functionality, the software rebuilds the position of the camera and determines their relative orientation. During this process, the algorithm extracts and matches the features in the images. It initializes with two images and subsequent images are added at the end of the sequence. Furthermore, BBA (Bundle Block Adjustment) is performed to reduce re-projection error. The lower error leads to higher quality of the resulting sparse point cloud, orthophoto and dense point cloud (Agisoft LLC, 2018).

4.2. Irradiance Compensation

The change in irradiance occurs because of the difference in the solar elevation angles and the change in relative distance of the sun. Bi-directional reflectance from the agricultural surface is non-Lambertian (not perfectly diffused) in nature i.e. the alteration in brightness due to the angle of view. The bi-directional reflectance effect also depends on the illumination conditions and is affected by varying intensity of subpixel shadows on the surface (Beisl & Woodhouse, 2004).

Illumination conditions change over time due to cloud cover, solar angle, atmospheric condition and the time of the day. This affects the amount of incoming radiation which consequently affects the radiance. Images taken within an interval of a few minutes may have variation in illumination condition. Irradiance compensation is done to reduce this effect of varied illumination conditions and to make the data comparable.

In dual sensor pair setting, as explained by Jin and Eklundh (2015), the reflectance (R) is computed by taking the ratio of the irradiance from the sunshine sensor (upward looking) and from the camera (downward looking). Since, there is constant bias in the calibration method because of the different angles of the sensors, it is resolved by introducing a constant factor (k), which is defined as,

$$R = \frac{I_C}{(k * I_S)} \qquad (1)$$

Where, I_C is the irradiance from the camera, I_S is the irradiance from the sunshine sensor, and k is computed as ratio of two sensors' sensitivities.

4.3. Radiometric Correction

The radiance recorded by the sensor mounted on the UAV may differ from the actual electromagnetic radiation reflected from the surface. Radiometric correction is a procedure in which the pixel values are calibrated to improve the quality of remotely sensed data resulting in approximately true reflectance values. This process is essentially important when images captured over different time period are compared. Omitting this process would result in reduced orthomosaic quality, inaccurate reflectance values and subsequently unreliable vegetation indices (Dunford, 2009; Mitchell, 2010; Wang & Myint, 2015).

The radiometric distortions are predominantly due to factors such as variations in the sensitivity of the sensors, differences in sun elevation and angle, uneven topography, and atmospheric interferences (Japan Association of Remote Sensing, 1999). Radiometric distortions are broadly classified as follows:

4.3.1. Distortions due to sensors

Variations in the functionality of the sensors due to degradation over time causes errors like bad pixilation, line or column dropouts and striping. Specifically, the sensors, which use optical lenses are vulnerable to vignetting, that is the fringe of the image appears darker than the center. Vignetting is caused due to the angle of the incoming rays to the optical axis of the sensor.

4.3.2. Distortions caused by variations in solar angle and the topography

Among the factors to be considered when performing UAV data collection are solar angle, viewing angle and topography. Solar angle and viewing angle causes variations in radiance. Solar angle and topography are the main elements that define Bi-Directional Reflectance Distribution Function (BRDF). BRDF simply explains the variations of radiance when the objects are viewed from different perspectives (i.e. angles).

4.3.3. Distortions caused by atmospheric interferences

Gases present in the atmosphere absorb and scatter solar radiations, which causes distortion in the images captured. Even though UAV imagery is not directly affected by the presence of clouds, the presence and the absence of clouds indirectly affect the images. On an overcast day, the light is diffused which may result in uniform/even reflectance. Whereas, on a sunny day, the condition of the light is sharp and it may result in glares on the surface. The atmospheric factors such as fog, presence of aerosols and BRDF also affects the captured images.

4.4. Sensor Calibration

Sensor calibration is performed in two ways: absolute and relative. In absolute calibration, the DN values of the image are transformed into surface reflectance values. On the other hand, in relative calibration, Lambertian reflectance panels with different degree of reflectance are used to normalize the sensor output (Guo et al., 2019). The more general and relatively simple method of sensor calibration is the Empirical Line Calibration (ELC). The ELC assumes that the relationship between the sensor radiance and the spectrally stable reflectance panels is linear (Clark, Suomalainen, & Pellikka, 2011a, 2011b). For ELC, it is important to select appropriate reflectance panels of different brightness.

Unlike traditional methods used for satellite imagery, UAV technology do not yet have a well-defined systematic method for radiometric calibration; therefore, further research is required to bridge this gap (Clemens, 2012; Wang & Myint, 2015).

4.5. Phenology and Vegetation Indices

Plants produce carbohydrates through photosynthesis utilizing water, carbon dioxide and sunlight. Chloroplast cells in the leaves contain the pigment chlorophyll that absorbs photons in the sunlight. This absorption is in the visible spectrum especially in the blue and the red bands (Grant, 1987). Healthier plants go through rapid photosynthesis and consequently absorb more radiation in the blue and the red parts of the spectrum; this behavior correlates with the health of chloroplast cells (Gausman, 1977). Healthy vegetation absorbs red and blue bands while reflecting NIR. On the other hand, stressed vegetation often have unhealthy and damaged chloroplast cells which tend to absorb less red light and also do not reflect as much NIR (SARE, 2019). The response curves for the healthy and stressed vegetations are shown in figure 4

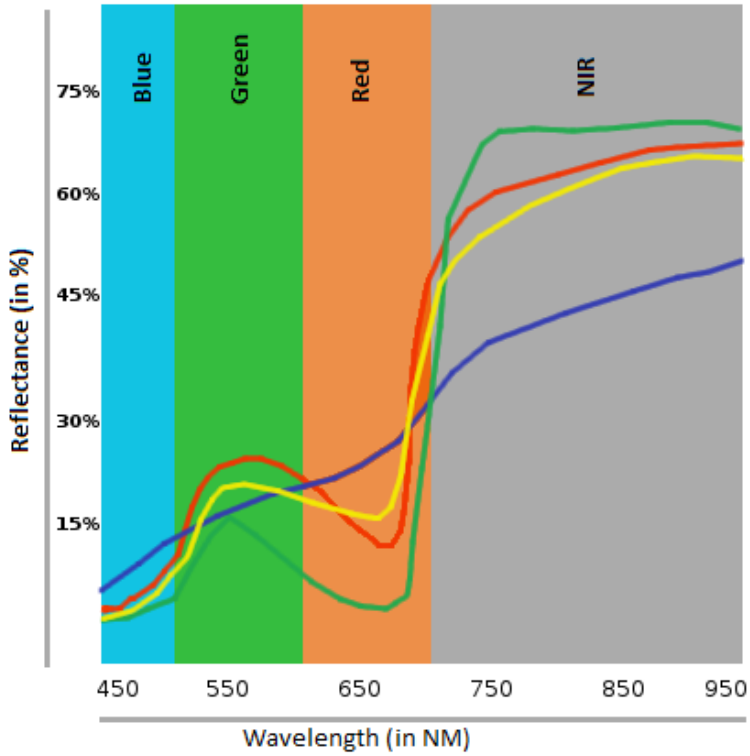

Figure 4: Spectral response curve for healthy (green), stressed (red), nitrogen deficient (yellow), and necrotic (blue) redrawn from SARE (2019).

This spectral response for plants sets it apart from it surrounding features (soil, water, etc) and allows use of metrics such as vegetation indices (VIs). The VIs are mathematical combinations of spectral bands indicative of plant characteristics. The primary usage of VIs is to indicate the amount of vegetation in terms of percentage cover for an area of interest (e.g., Leaf area Index (LAI), biomass, water use, plant health and crop production) (Jackson and Huete, 1991).

5. Methodology

5.1. Research Design

The descriptive correlational research design was employed for this research. This design explains the relationship between two phenomena where independent variables cannot be altered. Stangor (2019) defined descriptive correlational research as "A research designed to discover relationships among variables and to allow the prediction of future events from present knowledge." The design is chosen to statistically measure the relationship between variables. This is because relationships between crop yield/crop, biomass and vegetation indices are considered to be causal. In this study, the vegetation indices are independent variables which are assumed to be influenced by crop yield/ biomass. All the variables during the study are measured independently and are not altered. Broadly, the design involves measuring different variables and assessing the relationship between them. This is done without involving any changes to the independent variables.

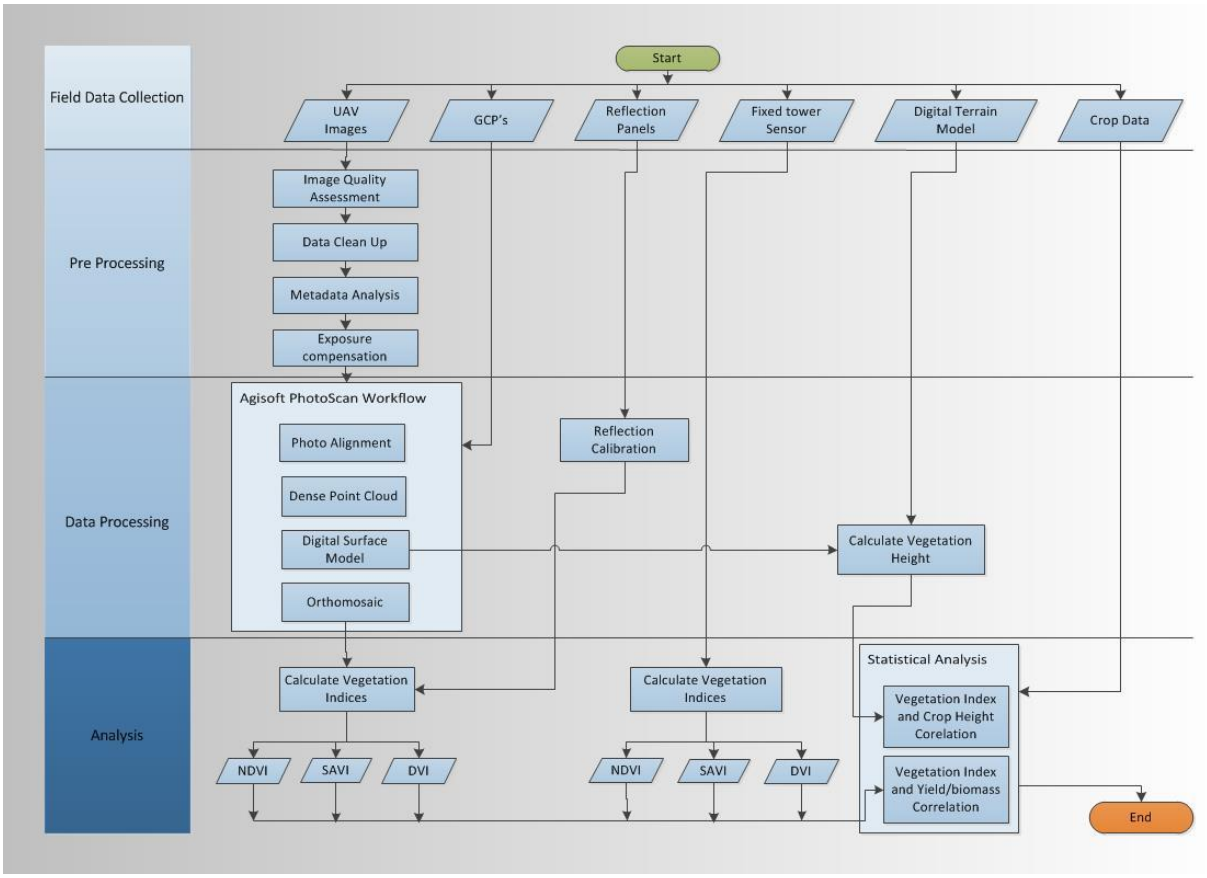

Figure 5: The flowchart shows the methodological framework incorporated in the study.

Since this study involved phenology of crops, the images captured at different time periods cannot be compared unless they are radiometrically corrected. In this analysis, radiometric corrections were performed manually by compensating for exposure and

reflectance. This radiometrically corrected dataset is used to calculate vegetation indices. The processing and analysis incorporated in the research is outlined in Figure 5.

5.2. Platform and Sensor

The data was collected using the following UAV: 3DR Solo quadcopter manufactured by 3D Robotics, Inc. (US).This UAV is displayed in Figure 6 and was fitted with a Parrot Sequoia multispectral camera as well as a sunshine sensor.

Figure 6: 3DR Solo UAV mounted with Parrot sequoia multispectral sensor and sunshine sensor. Photo: by Ashish Vivekar.

5.3. UAV Characteristics

3DR Solo quadcopter is considered as one of the first commercial smart UAV designed to capture aerial photos and video. The 3DR Solo has flight endurance of approximately 20 minutes when equipped with the sensors (payload 420 grams). Fully loaded solo weighs 1.8 kilograms including 500 grams of rechargeable smart lithium-polymer (li-po) battery (Anderson and 3DR staff 2015). Further specification of the 3DR Solo UAV is listed in Table 1.

Table 1: 3DR SOLO Specifications (Anderson and 3DR staff 2015)

3DR SOLO Specifications	
Flight time	25 minutes; 20 minutes with payload*
Range	0.5 miles (0.8 km)
Max speed	55 mph (89 km/h)
Max payload	420 g
Autopilot	Pixhawk 2
Frequency	2.4 GHz
Weight	3.3 lbs. (1.5 kg) / 3.9 lbs. (1.8 kg) with GoPro® and Solo Gimbal
Dimensions	10 in. tall (25 cm), 18 in. (46 cm) motor-to-motor

* Flight time varies with payload, wind conditions, elevation, temperature, humidity, flying style and pilot skill.

5.4. Sensor Characteristics

A Parrot Sequoia multispectral camera (Left, figure 7) with irradiance (sunshine) sensors (Right, figure 7) was used to capture images and acquire data for the study area. It is a lightweight camera specially designed to be mounted on small UAVs. This camera comes with an inbuilt GPS that records the location information and embeds a geotag to the recorded images. The multispectral camera captures four narrow bands of wavelength namely green, red, red edge and NIR. The sensor can provide information on the vegetation vitality by capturing the amount of light plants absorb and reflect. The green band indicates the chlorophyll content in the leaves, while the red band indicates variations in biomass and moisture. The Red edge indicates nutrient stress. Even though, all the bands indicate specific information, the NIR and red bands are most commonly used for studying plant characteristics since these wavelengths have contrasting characteristics of vegetation that is NIR wavelength has strong reflective properties while red has strong absorption (Parrot Sequoia, 2017). Specifications of these sensors are listed in table 2.

Table 2: Parrot Sequoia multispectral sensor and Irradiance sensor specification (Parrot Sequoia, 2017)

Specification	
Body	**Sunshine sensor**
4 spectral cameras	4 spectral sensors with the same filters (body)
Green: 530-570 nm **Red: 640-680 nm** **Red Edge: 730-740 nm** **Near Infrared: 770-810 nm**	GPS
Resolution: 1280 x 960	IMU + Magnetometer
Focal length 3.98 mm	
10 bits Global shutter	
Up to 1 FPS	

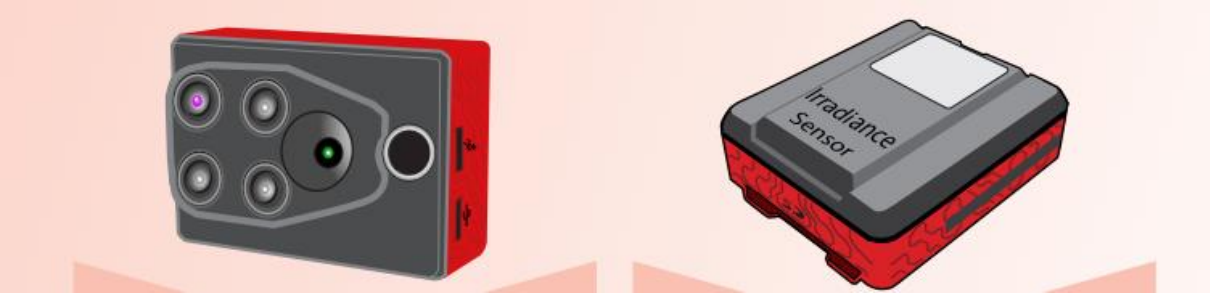

Figure 7: Parrot Sequoia multispectral sensor (left) and Irradiance sensor (right) (Parrot Sequoia, 2017).

5.5. Fixed Tower Sensor

Two downward looking sensors are attached to a 10-meter-high mast which is positioned between two plots. These sensors continuously monitored data from two different plots. The first sensor monitors a perennial wheatgrass crop called Kernza at approx. 264 degrees; the second sensor monitors an intercrop of Kernza and Lucerne at approx. 84 degrees, both of this upward and downward looking sensors record measurement every ten minutes in red (630 nm) and NIR (800nm) bands. The mast also holds upward looking radiance sensor. The timestamp of the data acquisition of the fixed tower sensor data and the UAV flight data are matched for optimum comparison purposes.

5.6. UAV Mission and Flight Plan

The UAV missions are planned and carried out by SITES officials as part of their regular monitoring program. The data for this study was collected six times throughout the growing season from 11th May 2018 to 17th September 2018. Favorable wind and lights conditions were taken into consideration so that less windy days with cloudy conditions were chosen for the flights as often as possible. Cloudy and overcast conditions provide diffuse light which reduces the glare and harsh shadows and thus reduces specular reflection (Maine, 2018). The study area is relatively windy throughout the year and requires a stable UAV, such as the 3DR Solo, and an experienced UAV pilot.

Mission Planner, a free open source and community supported software application was used to create the flight plan. The flight plan designed to attain 80% of front overlap and 75% of side overlap while maintaining a height of 60 meters from the ground. The average speed of the UAV is set at eight meters per second. The flight plan (as shown in Figure 8) is saved as waypoint mission and used for all the six flights. Figure 8 shows the UAV being deployed for the data collection. Each flight contains approximately 450 images. Before every flight, fixed GCP markers and reflective panels are placed in field with known coordinates and reflectance respectively for future reference.

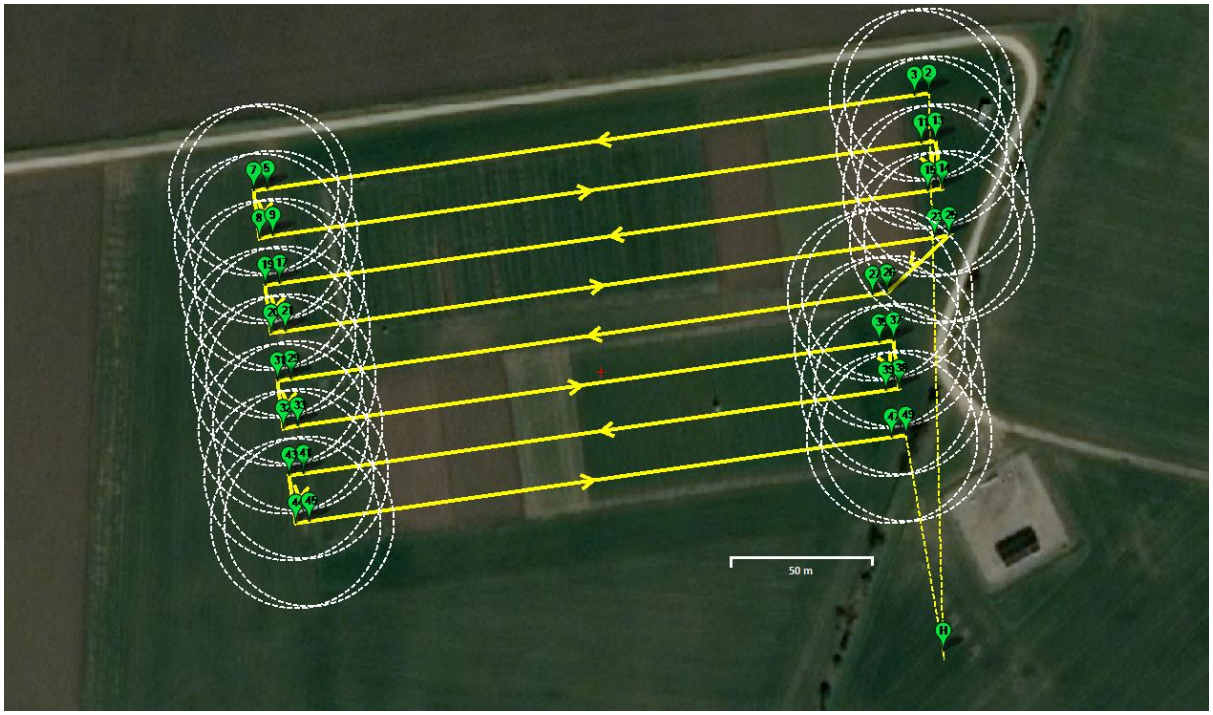

Figure 8: The figure shows the snapshot of flight plan created on Mission Planner software. Yellow line shows the path and direction of the flight, The basemap is from Google Earth.

Figure 9: Reflectance panels setup during actual UAV data collection mission at Lönnstorp..Photo: by Ashish Vivekar.

5.7. Ground Control Points

The study area had six evenly placed tiles which were used as GCPs. The distribution of GCPs that were used is depicted as red dots in Figure 10. The coordinates of the tiles were collected using high-precision RTK (Real Time Kinematics) device. The GCPs were measured in SWEREF 99TM coordinate system. Vertical coordinates were measured in RH2000 height system. The GCPs were consistent for all the flights and were marked with black and white chequered tiles. These GCPs were then used for geometric correction during the SfM process.

Figure 10: Marked GCPs overlaid on Google Earth (RGB) image dated (30th May 2018).

5.8. Reflectance Panels

Before each flight, three Labsphere's Spectralon® reflectance panels of different shades were placed on the field. These panels were cleaned and placed on a dark green tarp in such a way that they were not affected by shadows. The panel used were approximately 25 x 25 cm (10 x 10 inches), They need to be big enough to covers area several times of the pixel size of the sensor. It must be placed on the same elevation as the study area of interest and should exhibit high Lambertian reflectance standards (Smith & Milton, 1999). These reflectance targets have the property to diffuse incident light and maintain the contrast over the range of the illumination condition. These panels are ideal for post-flight reflectance calibration of the images. White, grey, and dark grey panels with the known reflectance of 50, 20, and 5 percent respectively were used in this study (see Figure 11).

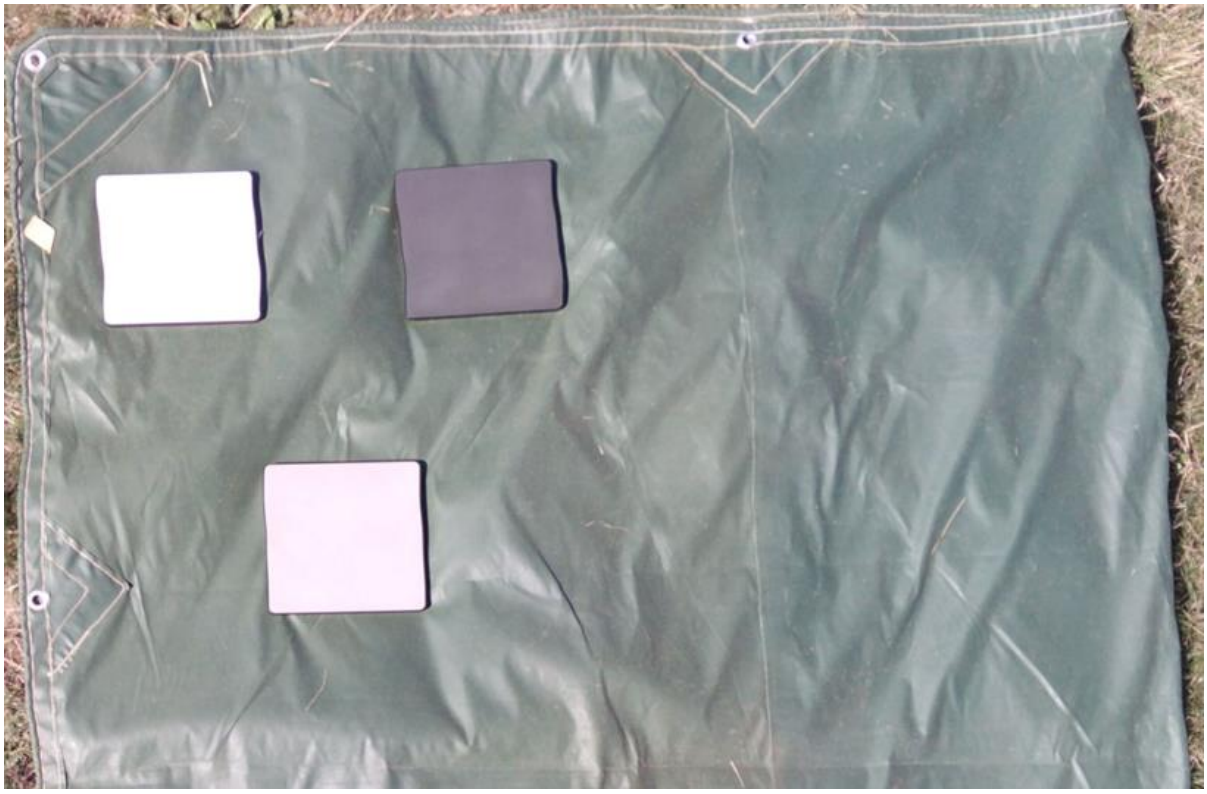

Figure 11: Reflectance Panels RGB image (Bright 50%, Dark 5% and Grey20%) RGB image from UAV. based on data from SITES.

5.9. Crops and Management

The observation regarding sowing date, fertilization and other management practices were recorded by the officials of SITES. The study area was divided into 25 small plots of various sizes; these plots are divided into 4 cropping systems as mentioned previously in the study area section (Section 3). The crop yield data was recorded per plot. Crop yield data were collected as fresh and dry weight (in kg/ha).

In case of legume lay and sugar beet, both the fresh and dry yields were recorded, whereas only dry weight data was recorded for all other crops. Samples of legume ley were collected from patches of 0.25 square meters area from each of these 9 plots. The total weight of the fresh and the dry biomass were recorded for the first harvest, whereas, for the second harvest the fresh and the dry weight of legume ley grass, clover, and weeds were recorded separately. To maintain consistency in the analysis, only total fresh and total dry biomass is used from both the harvests of legume ley.

While, in case of other crops (spring wheat & faba bean, winter wheat, spring barley & lupine, spring barley, winter oilseed rape, wheatgrass (Kernza) and Kernza & Lucerne) dry weight of straw and kernels were measured from patches of one square meter. Only in case of sugar beet, samples were collected from two rows of eight meters with area of 7.68 square meters.

5.10. Software Application

Agisoft Photoscan was the software package used for generating orthomosaics and dense point clouds from drone imagery. ENVI, Python IDE and MATLAB were used for performing radiometric corrections. Microsoft Office was used for data visualization, data management and writing the report. Google Earth and mission planner applications were used for making the flight plan and visualization.

5.11. Image Processing

5.11.1. Data Cleanup and Metadata Analysis

The entire dataset was manually checked for quality (corrupt, blurred and dark images). For pre-processing, the data was cleaned and sorted. The images taken during landing and takeoff (where altitude was lower than usual flying height) were identified and discarded as takeoff and landing were manually handled to take pictures of reflectance panels, Apart from this, blurred and distorted images and images from the diagonal path (to improve efficiency while performing solar angle compensation) were identified and deleted.

5.11.2. Exposure Compensation

The image dataset collected at different times was exposed to different illuminating conditions. For optimum comparison it was particularly important to calibrate the data sets. The factors influencing exposure are overcast conditions, changes in International Organization of Standardization (ISO also known as film speed), aperture size, shutter speed, and solar angle. For data collection, the sensors aperture size was set to static; however, the ISO and the shutter speeds were set to automatic. The ISO was relatively stable but shutter speed (also called as exposure time) varied from 0.001 to 0.0001 seconds. Especially, in case of narrow Red-Edge band (730–740 nm), the shutter speed was quite slow (approx. 0.001 seconds), except in the case of the July dataset.

In this study, each dataset consisted of about 450 multispectral images. To generate high accuracy mosaics, even the slightest variations in illumination between image tiles was considered and compensated accordingly. The variations arose because of changes in direction of flight and different composition of each frame. The most effective way to adjust the effect of illumination would have been to set a constant value of exposure for each image before it was taken. However, this was not possible since the setting in Parrot Sequoia does not permit to have only shutter speed as automatic. The system either permits to have all settings (shutter speed, aperture and ISO) fixed, or the aperture fixed while the ISO and the shutter speeds can be automatic. The preset automatic shutter speed in the Parrot Sequoia could not be changed without changing the ISO. To compensate for differences in the exposure setting when the images were taken, it was decided to normalize the relative exposure of every image. In other words, we selected exposure value from one image in the

dataset and adjusted all other images by compensating for the changes in shutter speed and the ISO of the selected image. The exposure compensation for this step was evaluated using Equation 2.

$$DN_{EC} = DN * \frac{k^2}{\tau K} \quad (2)$$

Where,

k is the aperture F number, τ is the exposure time in seconds, K is the ISO of the multispectral sensor, and DN is Digital number.

5.11.3. Orthophoto Generation

Orthophotos and DEM (Digital Elevation Model) are generated using Agisoft PhotoScan Professional (Agisoft LLC) version 1.3.2. Images gathered via UAV sensors were imported into the application. The camera position for all the images were aligned to build the sparse point cloud with high accuracy. For precise geo-referencing, accurate model construction and further optimization, camera positions of the 6 GCP markers were used. To make the process quicker, we created mesh enabling the software to guide us near the probable place of markers so that we can easily locate GCP on the photo to place the marker. To achieve even higher accuracy in calculating the internal and external parameters of the camera, it was recommended by the user manual of the software to use the 'Optimize Camera Alignment' setting. This step is suggested if GCP coordinates are known precisely. Generally, the SfM algorithms require high computing power. Even with a powerful workstation (Intel core i7-6700 @ 3.40Ghz with 64 GB RAM), it took 5-8 hours to process one data set (processing time depends mostly on the hardware configuration). Batch processing was used to run multiple commands concurrently. This process resulted in dense point cloud, DEM, and orthomosaic for each dataset.

5.11.4. Reflectance Correction and Calibration

For the purpose of this study, Empirical Line Correction (ELC) was used; this is a target-based reflection correction method. This approach calibrates digital numbers at sensor irradiance for each band with reflectance coefficient of the targets. By using reflectance panels of known reflectance in the field the reflectance values and observed values were compared and subsequently the data was normalized accordingly. The reflectance factors will have a linear relationship with the reflectance panels of different reflectance (here 50%, 20% and 5%) for each band. Using the reflectance targets, the absolute reflectance values were calculated; this enabled comparing the data captured during different flights.

The reflectance values collected by cameras from reflectance panels are prone to errors due to the inability to compensate for the position of the Sun relative to the target and the sensor. Relative position of the sun changes with the time of the day as well as with the time of the year.

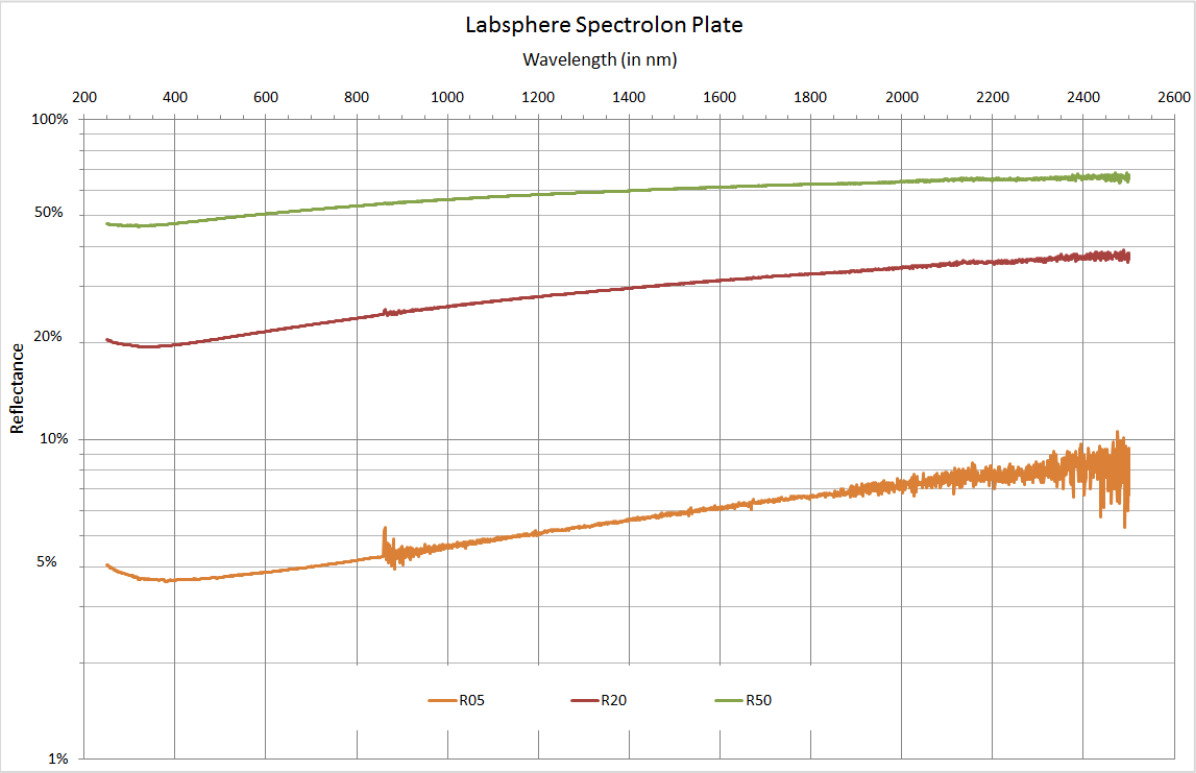

Figure 12: Wavelength dependence of reflectance for the reflectance panels (Plotted by Dr. Hong Xiao using Spectralon Documentation).

Generally, the optical properties of the Spectralon panels make them optimal for measuring canopy reflectance and BRDF correction; It supports the detection of the effects of emitted light other than surface properties (Georgiev & Butler, 2007). In this study, the wavelength dependent reflectance values measured from three Spectralon panels of varying brightness from 5% (bright), 20% (grey) and 50% (dark grey) were used. The reflectance variation of the panels for varying brightness of the panels is depicted in Figure 12 as shown above. The reflectance values of the panels are used as per the documentation of the Spectralon. The true reflectance values for the panels in various bands are mentioned in Table 3. When the reflection values are close to saturation i.e. DN value above 60000, it may lead to unreliable results. Therefore, it was decided to discard the DN values which were above 60000; only unsaturated values were used for developing regression models. In some cases, it was observed that the values of band 1 (green) and band 2 (red) reached its saturation limits. The values for bright (0.5) panel from band 1 and band 2 from all six datasets were discarded to maintain consistency. Consequently, the values from dark grey (0.05) and grey (0.20) panels were used to calculate regression models for band 1 (green) and band 2 (red) while

values from all three reflectance panels were used for generating regression models for band 3 (red edge) and band 4 (NIR). These regression models were then used for band wise reflectance calibration for each image using values listed in table 3.

Table 3: Band-wise reflectance of Labsphere Spectrolon Plate

Known Reflection				
	Band 1 Green (550nm)	Band 2 Red (660 nm)	Band 3 Red-Edge (735 nm)	Band 4 NIR (790 nm)
Bright Panel (50%)	0.4991	0.5167	0.5281	0.5357
Grey Panel (20%)	0.2121	0.2240	0.2322	0.2381
Dark Panel (5%)	0.0377	0.0393	0.0406	0.0416

In figure 13, the regression lines show the dependency between DN values by the UAV-based sensor and the reflectance values of Spectralon Panels measured for each band (red, green, red edge and NIR). Three Spectralon panels representing different light intensities were used. These are noted with **B**(right), **G**(rey) and **D**(ark) and correspond to the light reflectance of 50%, 20% and 5%, respectively. The DN values were taken from the images captured on 11 May 2018. Similar relationships were computed for the flights conducted on 13 June 2018, 26 July 2018, 21 August 2018, and for the flights on the 4th and 17th of September 2018, respectively. The graphs for the corresponding relationships are mentioned in the appendix section B (figure B1-B6).

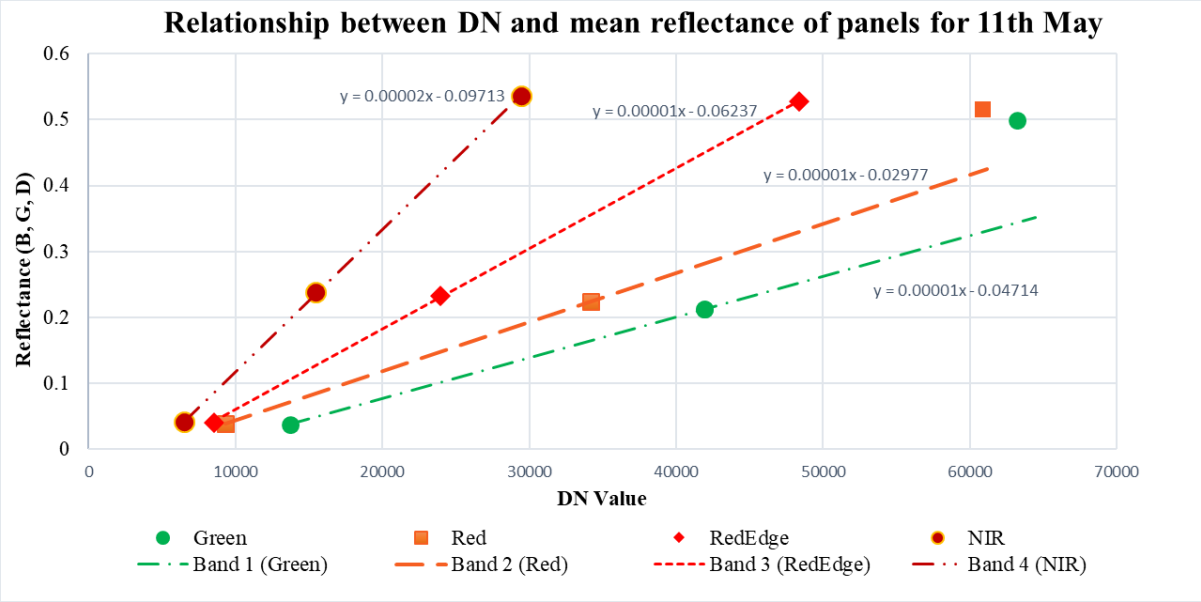

Figure 13: Correspondence between DN values at Sensor (UAV multispectral) and reflectance based on Spectralon Documentation.

5.12. Vegetation Index Calculation

5.12.1 NDVI (Normalized Difference Vegetation Index)

NDVI is the most commonly used index of vegetation greenness and photosynthetic capacity (Walker et al. 2012). It is a simple numerical indicator for remotely measuring the reflectance pattern of green vegetation 'greenness' from an aerial platform (Rouse Jr, Haas, Schell, & Deering, 1974). The index assesses the presence of vegetation in the target area by using red and near infrared bands (NIR) of electromagnetic radiation. This particular combination of the bands was chosen for the normalized difference formulation which uses one band (red) of the strong absorption and one band (NIR) of high reflectance/weak absorption of chlorophyll (Gitelson, 2004). The index, however, tends to saturate at high values of leaf area index (LAI). High values of LAI can be characterized by dense vegetation, especially, during leaf production and leaf senescence periods (Wang et al. 2005). The usual range of NDVI values are from -1 to 1 in where negative values represent water bodies, values close to 0 represents snow, rock, sand or bare soil; and positive values between 0.1 – 0.3 represents shrubs and grasslands; while higher values represent dense forests (Pinzon & Tucker, 2014; Tucker et al., 2005). The absolute value of NDVI are sensor specific and direct comparison between NDVI measured from different sensors may not yield correct results (for e.g. AVHRR and MODIS sensors may have different NDVI values for the same location). In general, higher vegetation density corresponds to higher NDVI values. Additionally, unhealthy and sparse vegetation reflects more red and less NIR than healthy and dense vegetation; whereas, bare soil reflects moderately in both red and infrared and results in lower values (Rouse Jr et al., 1974). Mathematically, NDVI is computed using the following equation (Equation 3).

$$NDVI = \frac{(NIR - Red)}{(NIR + Red)} \qquad (3)$$

5.12.2 SAVI (Soil-Adjusted Vegetation Index)

The background soil reflectance can considerably influence NDVI values (Epiphanio and Huete 1995) by up to 20%. To ascertain if NDVI values were influenced by background soil, SAVI is calculated. This index is similar to NDVI, but it helps to overcome the effects of soil brightness. Soil color, soil moisture, and other properties of the soil influence the spectral properties of the vegetation. SAVI attempts to minimize the effect of background soil brightness by using a canopy background adjustment factor, L, which is a function of vegetation density representing the proportion of vegetation in a certain area. It often requires prior information about the area's vegetation amounts being analyzed.

Huete (1988) suggests an optimal value of L=0.5 to account for the first-order soil background variations. This index is best used in areas with relatively sparse vegetation where soil is visible through the canopy. The general equation for SAVI is computed as follows in equation 4.

$$SAVI = \frac{(1+L)(NIR-Red)}{(NIR+Red+L)} \quad (4)$$

SAVI is usually used in areas where vegetative cover is low (< 40%). The adjustment factor values i.e. L ranges from 0 to 1; where 1 is very high vegetation and 0 is very low vegetation. In general, value of 0.5 (L = 0.5) is used for intermediate vegetation cover. The precise value of L can be arrived at by trial and error. It is calculated as a factor which gives equal VI values for dark and light soils. The value of L=0.5 was selected for this research. Consequently, the general equation is represented by equation 5.

$$SAVI = \frac{1.5*(NIR-Red)}{(NIR+Red+0.5)} \quad (5)$$

5.12.3 DVI (Difference Vegetation Index)

This index is very sensitive to the amount of vegetation and readily distinguishes background soil from vegetation (Mróz & Sobieraj-Żłobińska, 2004). Similar to NDVI and SAVI, in DVI, zero indicates bare soil, values less than 0 represents water, and those greater than 0 represents vegetation. The DVI is evaluated using the equation 6 as represented below (Tucker, 1979).

$$DVI = NIR - Red \quad (6)$$

5.13. Vegetation Height Calculation

Vegetation height is calculated as the difference between the bare earth surface model (DTM) and the Digital Surface Model (DSM) and represented as the Crop Surface Model (CSM) as depicted in Figure 13. Ideally, the DTM should have been extracted from the dataset when there are no crops in the field. Since such dataset was unavailable, it was decided to use previously available datasets. The datasets were analyzed based on the harvest dates and the visual inspection. Plots with no plant cover were selected for extracting the terrain model. The DTM was generated using the points from the plots with bare soil. The same surface was extrapolated for the whole study area with the assumption that the study area is flat and uniform.

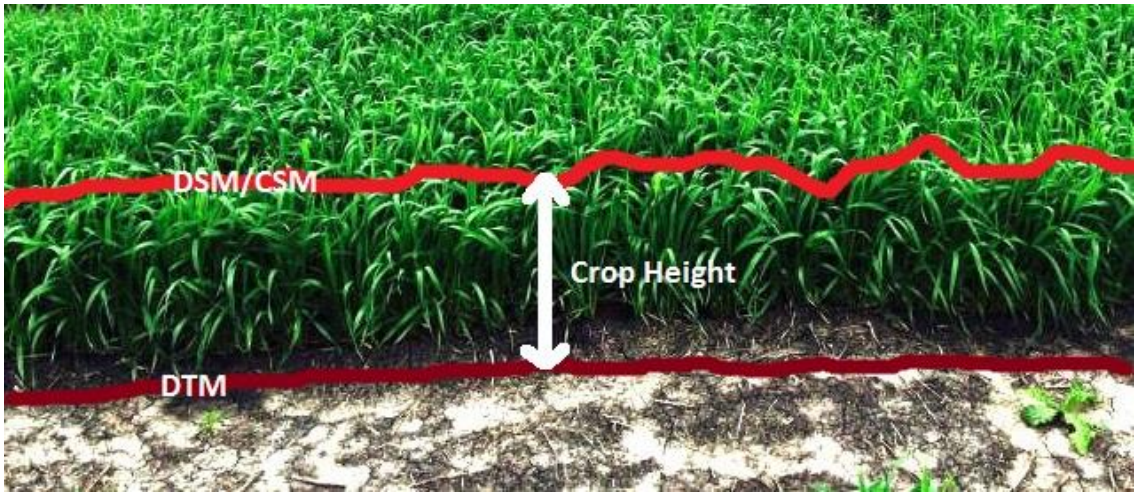

Figure 14: Crop height is calculated as the difference between DTM and DSM extracted from dense point cloud.

The image captured from each flight data provided the corresponding surface models referred to as CSMs. To measure the height of the crops, the difference between the CSM and DTM is calculated (Figure 14). This facilitated analyzing the variation of crop growth spatially and temporally. The height of the crops at each flight date was calculated from CSMs of different dates. These crop heights were then used for establishing the associations with vegetation indices; the findings of which is mentioned in the result section.

5.14. Correlation Analysis

Broadly, 'correlation is used to refer to an association, connection, or any form of relationship, link or correspondence' and statistically how two variables co-vary. The usual range varies between -1 to 1, where -1 indicates perfect negative correlation, 0 indicates no correlation, and 1 indicates perfect positive correlation (Mukaka, 2012). Pearson and Spearman correlation coefficients were calculated for crop yields and the vegetation indices to identify the dynamics between them. Pearson and Spearman correlation were selected because these provide insights about the relationship (monotonic or linear). While a full significance test was not performed, the results were interpreted using a general rule (Hinkle, Wiersma, & Jurs, 2003) as described in table 6. The size and the sign of the coefficient indicate the degree and the direction of the correlation respectively.

Table 4: Correlation coefficient and its interpretation general rule by Hinkle et al., (2003).

Size of Correlation	Interpretation
0.90 to 1.00 (- 0.90 to - 1.00)	Very high positive (negative) correlation
0.70 to 0.90 (- 0.70 to - 0.90)	High positive (negative) correlation
0.50 to 0.70 (- 0.50 to - 0.70)	Moderate positive (negative) correlation
0.30 to 0.50 (- 0.30 to - 0.50)	Low positive (negative) correlation
0.00 to 0.30 (0.00 to - 0.30)	Negligible correlation

6. Results

This section presents the results of the analysis.

6.1. The radiometrically corrected multispectral UAV imagery showed similar trends of NDVI, SAVI and DVI with the one computed from the fixed tower sensors. The processed values for the chosen vegetation indices from UAV sensor as well as sensors placed at the tower for plot 25 (Sensor on tower record reflectance for this plot only) is presented in the figure 15, 16 and 17 respectively. These figures suggest that UAV sensor overestimated the vegetation indices in general and there was stable offset between these two (UAV and fixed tower sensor). Following figures also depict high inter day variation in fixed tower sensor readings (blue points) especially in the month of May, June and August.

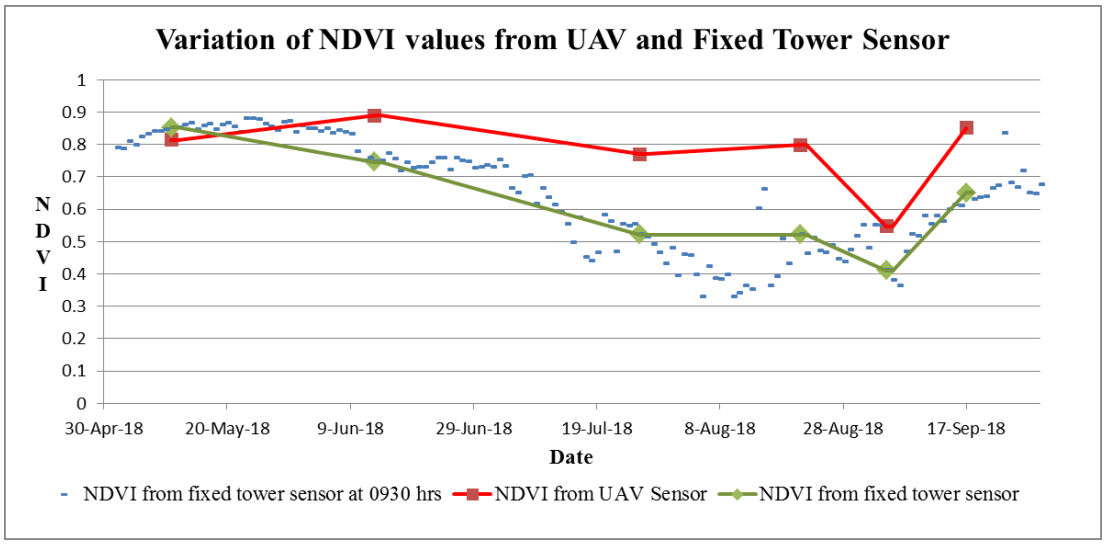

Figure 15: Variation of NDVI values from UAV and Tower Sensor.

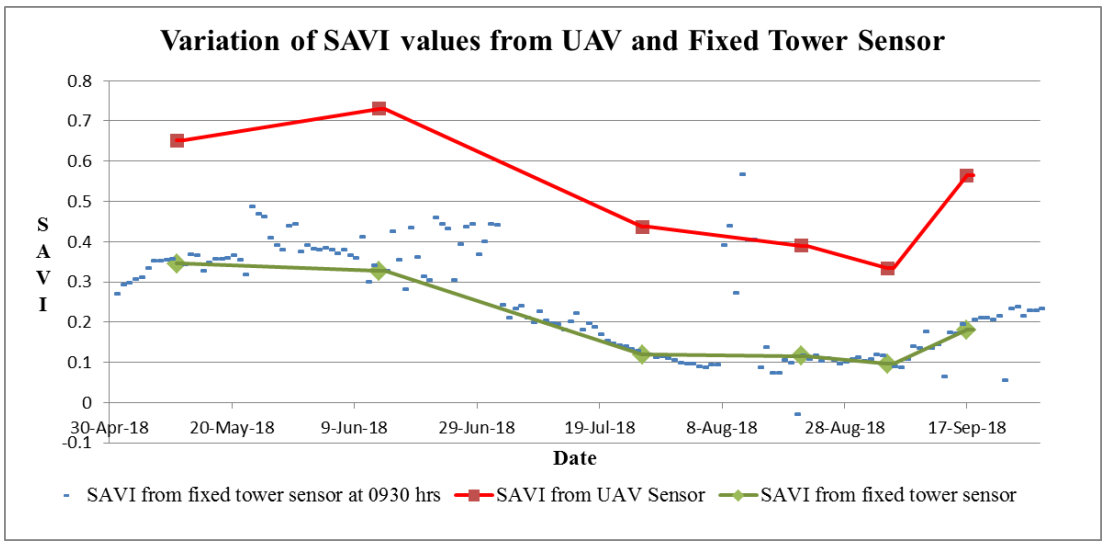

Figure 16: Variation of SAVI values from UAV and Tower Sensor

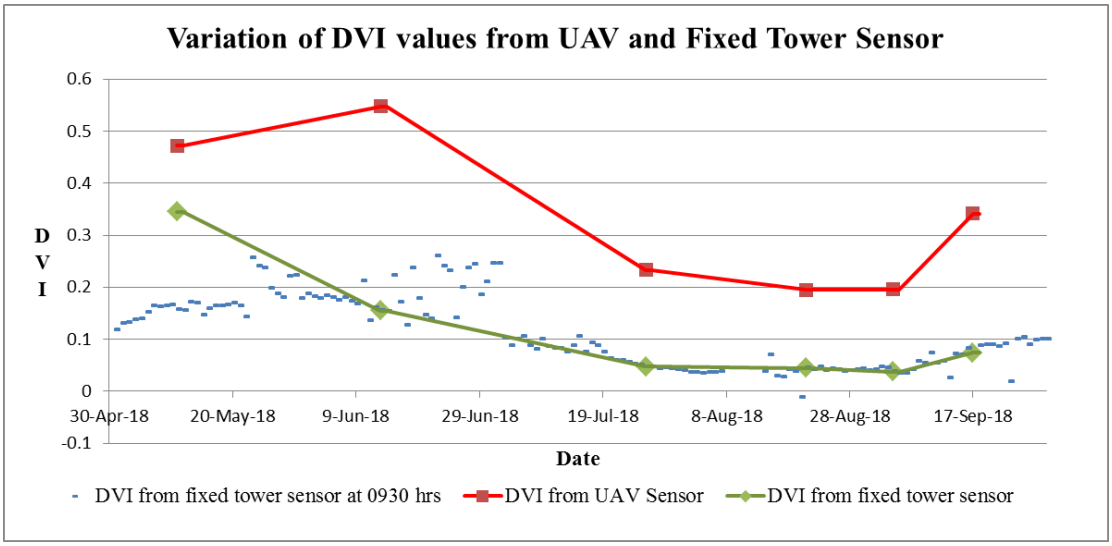

Figure 17: Variation of DVI values from UAV and Tower Sensor

Having considered the consistent pattern of overestimation, the correlation of VIs obtained from both sensors shows very high association (r>0.85) as shown in Table 5. Surprisingly, SAVI from UAV sensor exhibits very high correlation with all three VIs from fixed tower sensor.

Table 5: Correlation between VI values obtained from tower sensor and UAV sensor Data

	NDVI Fixed Tower	**SAVI Fixed Tower**	**DVI Fixed Tower**
NDVI from UAV sensor	**0.86**	0.67	0.63
SAVI from UAV sensor	0.90	**0.94**	0.93
DVI from UAV sensor	0.85	0.94	**0.95**

Besides comparing the vegetation indices from the two sensor platforms an attempt was also made to perform correlation analysis of crop heights with selected vegetation indices. The plant height obtained from CSM of each plot was correlated with mean VIs of respective plots; the results are tabulated in Table 6. Scatterplots in Figures 18, 19 and 20 illustrate the relationship of crop height with specific VIs on 3 different dates. Scatter plots for remaining relationships are provided in appendix section D (Figure D1, D2 and D3).

Table 6: Correlation between crop height and vegetation indices

	Average Plant Height					
	11th May	13th June	26th July	21st August	04th Sept	17th Sept
NDVI	0.51	0.47	0.65	0.19	0.73	0.87
SAVI	0.57	0.72	0.45	0.04	0.74	0.85
DVI	0.62	0.80	0.19	-0.02	0.73	0.81

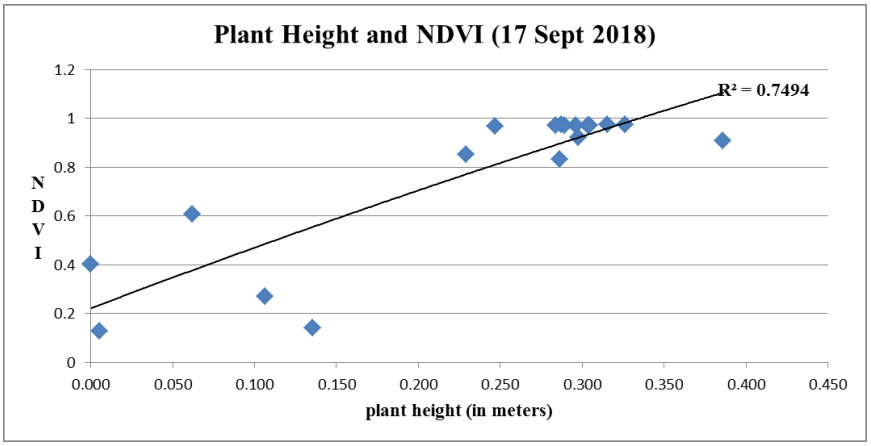

Figure 18: Scatter plot of plant height vs NDVI (calculated from dataset of 17th September 2018) n=18.

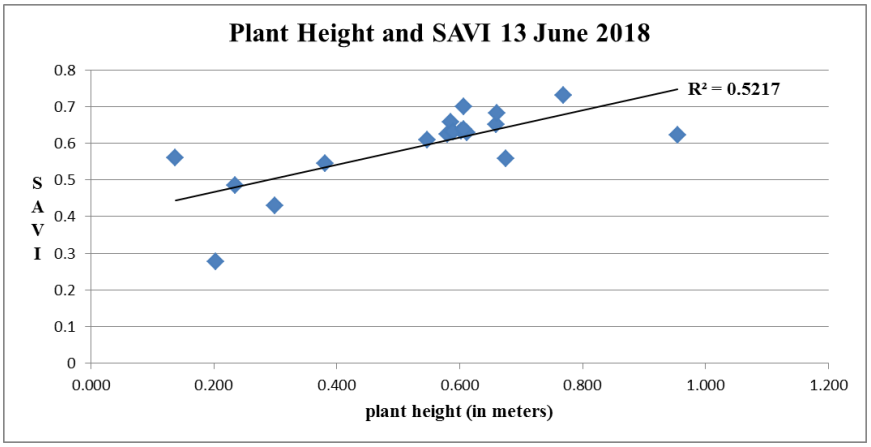

Figure 19: Scatter plot of plant height vs SAVI (calculated from dataset of 13th June 2018) n=18.

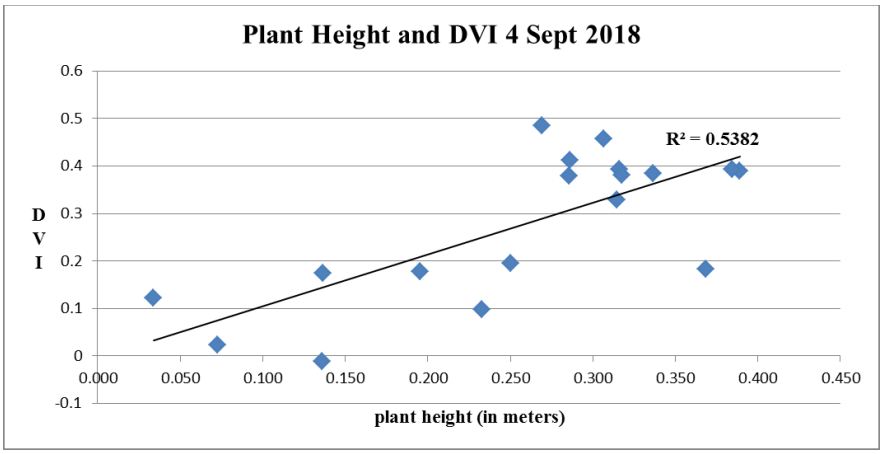

Figure 20: Scatter plot of plant height vs DVI (calculated from dataset of 4th September 2018) n=18.

Moderate to strong positive correlation between plant height and vegetation index was observed in all cases except for the data collected on 21 August 2018. As most of the crops were already harvested on that date, and could partly explain the low correlation values than other dates.

6.2. To answer our second research objective 'to identify the relationship between VIs derived from multispectral UAV imagery and crop yield of selected crops in a Swedish agricultural area', we tested correlation between them.

For clarity and consistency of results, categories were defined based on the crop type and the harvest date. 18 plots of crop were classified into two groups. All the nine plots with Legume ley were grouped together as 'Legume ley' and remaining nine plots were grouped as 'Other crops'. Legume ley plots were harvested twice in the growing season and yield was measured after each harvest. The yield from first harvest and second harvest are labelled as 'first harvest' and 'second harvest' respectively. The yield weight measurements were taken for fresh as well as dried crops and labelled as 'Fresh weight' and 'Dry weight' respectively. Other crop plots were classified again on the basis of harvest dates. They were grouped into 3 subcategories: i) All crops (except Legume ley) ii) Remaining crops harvested before 26 July 2018 and iii) Remaining crops harvested between 26 July 2018 and 21 August 2018.

Table 7 shows the correlation coefficients (Spearman and Pearson) for all plots of Legume ley (n=9). Since, the first harvest was on 25 June 2018, the yield from the first harvest with the VI values calculated from the flight data before harvest was used. Similarly, for the second harvest, the VIs calculated from flights between the first harvest and second harvest were used.

Table 7: Correlation analysis between Legume ley yield (first harvest) and corresponding vegetation index (9 plots).

First Harvest			
NDVI		11th May	13th June
Fresh weight	Spearman	0.62	0.00
Dry weight	Spearman	0.58	-0.10
Fresh weight	Pearson	0.39	0.22
Dry weight	Pearson	0.17	0.05
SAVI			
Fresh weight	Spearman	0.63	0.17
Dry weight	Spearman	0.55	0.07
Fresh weight	Pearson	0.35	0.30
Dry weight	Pearson	0.05	-0.01
DVI			
Fresh weight	Spearman	0.45	0.25
Dry weight	Spearman	0.30	0.10
Fresh weight	Pearson	0.31	0.27
Dry weight	Pearson	0.01	-0.06

In the case of the first harvest, the VIs calculated from the flight conducted on 11 May 2018 show moderately strong positive correlation with the yield. The stronger relationship (bigger correlation coefficients) indicates greater association between variables. The Spearman correlation coefficients were consistently stronger than the Pearson correlation coefficients and indicated the monotonic type of relationship between variables. Conversely, very weak relationship was observed when comparing the yield with the VI result of 13 June 2018. Furthermore, the relationship was slightly stronger for the 'fresh weight' as compared to that of the 'dry weight' as shown in Table 7.

On the other hand, for the second harvest of the Legume ley, the best relationship (characterized by correlation coefficient) was found in the beginning of the growing season i.e., on 26 July 2018 as mentioned in Table 8. A moderately strong positive correlation between VIs and crop yield for Pearson and slightly less positive correlation for Spearman was observed. In contrast to the first harvest, Pearson correlation was observed to be consistently higher than the Spearman correlation indicating a higher linearity in the relationship of the variables. Surprisingly, the VIs measured in the month of August showed moderately negative correlation (Pearson and Spearman) with both the fresh and the dry yield. Weak relationship was detected for the rest of the dates.

Table 8: Correlation analysis between Legume ley yield (second harvest) and corresponding vegetation index (9 plots).

Second Harvest					
NDVI		26th July	21st August	04th September	17th September
Fresh weight	Spearman	0.25	-0.38	0.17	-0.12
Dry weight	Spearman	0.35	-0.38	-0.12	-0.05
Fresh weight	Pearson	0.57	-0.49	0.42	-0.11
Dry weight	Pearson	0.55	-0.49	0.30	-0.17
SAVI					
Fresh weight	Spearman	0.53	-0.43	0.08	-0.15
Dry weight	Spearman	0.40	-0.47	-0.17	-0.13
Fresh weight	Pearson	0.78	-0.52	0.37	0.02
Dry weight	Pearson	0.63	-0.55	0.25	-0.15
DVI					
Fresh weight	Spearman	0.62	-0.47	0.10	0.03
Dry weight	Spearman	0.43	-0.50	-0.15	0.00
Fresh weight	Pearson	0.77	-0.45	0.37	0.04
Dry weight	Pearson	0.60	-0.52	0.26	-0.14

By visual inspection we identified some patches in the Legume ley plots which looked very distinct but upon enquiry with the staff of SLU, it was found that a faulty sowing machine caused it. These patches were observed in all the six datasets for all the flight dates as seen in the Figure 21 for 11 May 2018. These three affected plots were omitted from the further analysis. Images of other dates can be seen in appendix section C Figure C1.

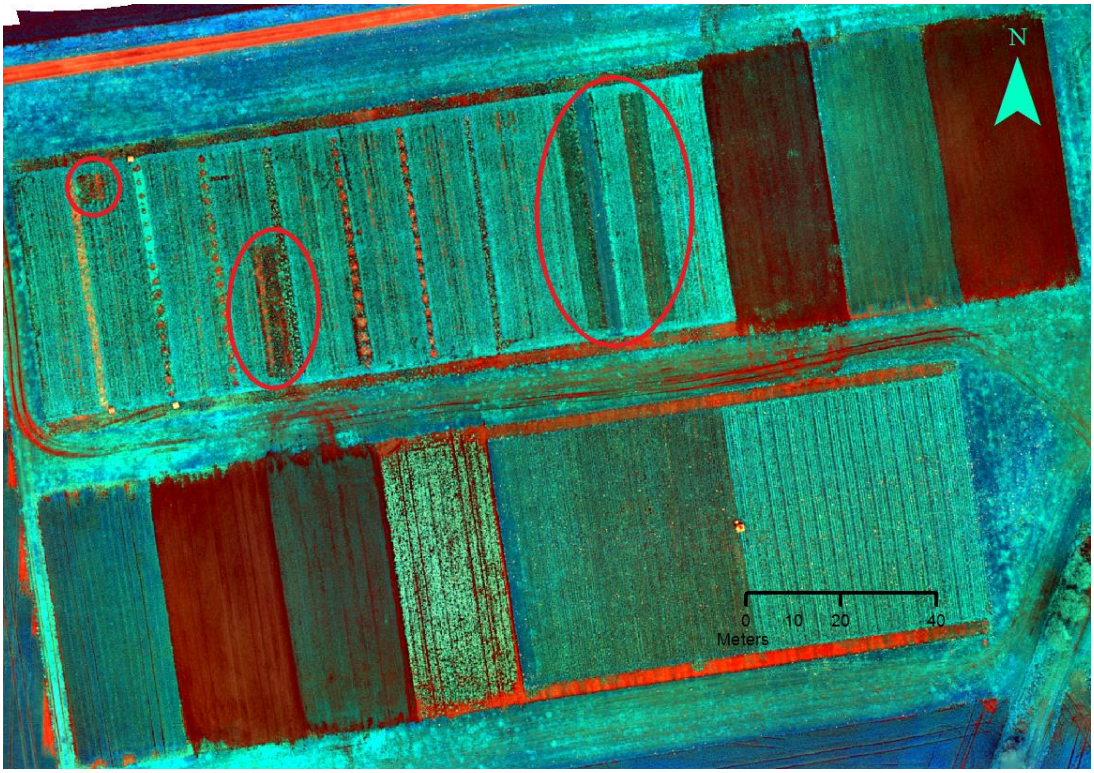

Figure 21: Orthomosaic of the study area in false colour composite (11th May 2018), the patches are marked with red.

The omission of these 3 affected plots improved the correlation coefficients (Spearman and Pearson); the improvements are seen in Table 9 and 10. Spearman correlation coefficient was higher than Pearson in all the cases (except in the case of Fresh weight with NDVI) indicating monotonic relationship.

Table 9: Correlation analysis between Legume ley yield (first harvest) and corresponding vegetation index after the removal of affected plots.

First Harvest			
NDVI		11th May	13th June
Fresh weight	Spearman	0.77	-0.49
Dry weight	Spearman	0.77	-0.37
Fresh weight	Pearson	0.80	-0.35
Dry weight	Pearson	0.72	-0.23
SAVI			
Fresh weight	Spearman	0.89	0.03
Dry weight	Spearman	0.66	-0.03
Fresh weight	Pearson	0.65	-0.10
Dry weight	Pearson	0.45	-0.13
DVI			
Fresh weight	Spearman	0.60	0.26
Dry weight	Spearman	0.26	-0.09
Fresh weight	Pearson	0.55	0.24
Dry weight	Pearson	0.32	0.05

The coefficient of determination, R^2, tells what percent of the variation in data values is explained by the regression line. For fresh yield of legume lay, NDVI can explain about 64% of variation from 11 May dataset whereas for dry yield the 51% variation is determined by regression line as seen in the Figure 22.

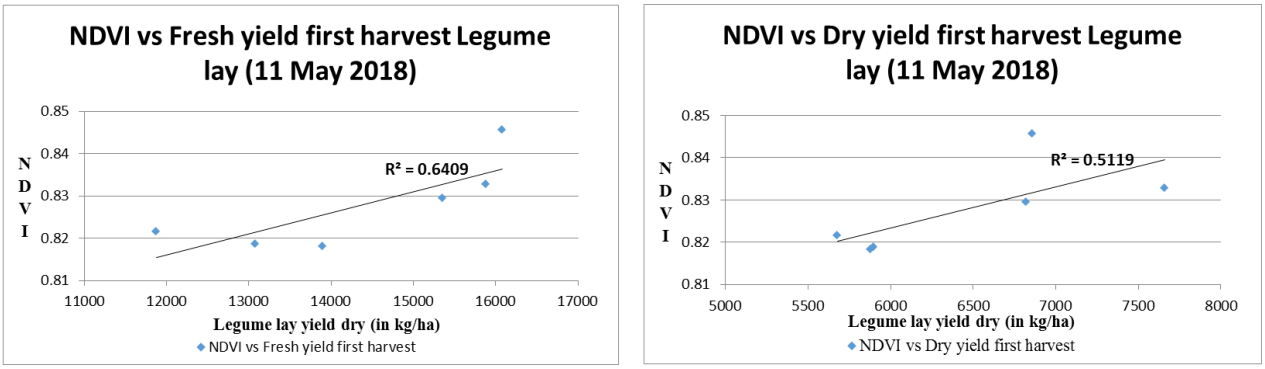

Figure 22: Sample scatterplot for first harvest legume lay yield fresh (left) and dry (right) with NDVI of 11th May 2018, n=6.

For the second harvest, the results are remarkably similar to the first harvest but with slightly stronger correlation for the yield with all three VIs. The data from 26 July 2018 had the highest positive correlation. The data from the 21st August 2018 exhibited moderately strong negative correlation with the Pearson coefficients being slightly stronger as seen in table 10 below.

Table 10: Correlation analysis between Legume ley yield (second harvest) and corresponding vegetation index, after removal of affected plots.

Second Harvest					
NDVI		26th July	21st August	04th September	17th September
fresh weight	Spearman	0.49	-0.26	0.20	-0.09
Dry weight	Spearman	0.37	-0.60	-0.26	-0.14
fresh weight	Pearson	0.63	-0.61	0.45	-0.24
Dry weight	Pearson	0.45	-0.84	0.25	-0.47
SAVI					
fresh weight	Spearman	0.77	-0.26	0.20	0.14
Dry weight	Spearman	0.54	-0.60	-0.26	0.14
fresh weight	Pearson	0.79	-0.59	0.48	0.19
Dry weight	Pearson	0.56	-0.82	0.29	-0.09
DVI					
fresh weight	Spearman	0.71	-0.26	0.20	0.31
Dry weight	Spearman	0.37	-0.60	-0.26	0.26
fresh weight	Pearson	0.78	-0.49	0.51	0.26
Dry weight	Pearson	0.56	-0.74	0.31	-0.01

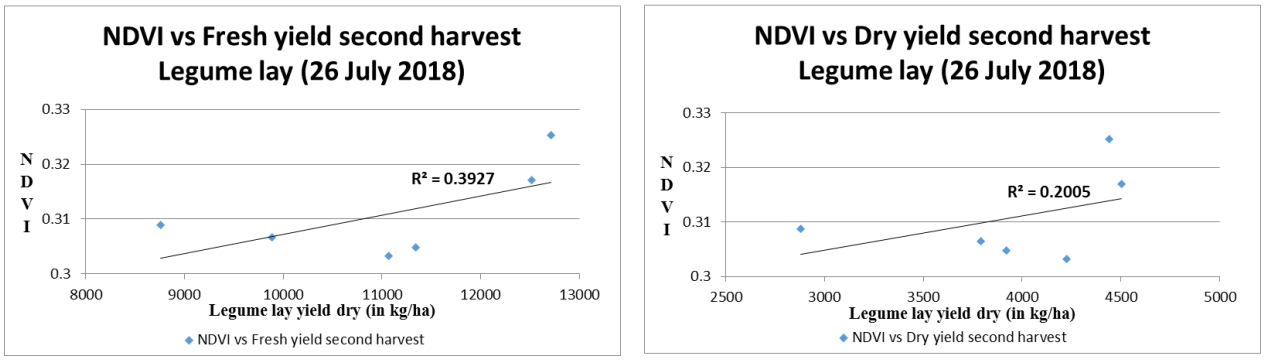

Figure 23: Sample scatterplot for second harvest legume lay yield fresh (left) and dry (right) with NDVI of 26th July 2018, n=6.

For all other crops, which consist of Faba bean/Spring wheat, Winter wheat/Insowed ley, Spring barley/Lupine, Winter wheat, Sugar beet, Spring barley, Oilseed rape, Kernza and Kernza/Lucerne on a single plot each, only the dry weight measurements were taken. Table 11 describes the Spearman and Pearson correlation coefficients between dry weights (yield) of these crops with their corresponding VIs. Both correlation values exhibit a very strong positive correlation in both the datasets of September when almost all the crops were already harvested. These results are considered unreliable since the yield data is based on the crops which are harvested; whereas, the vegetation indices are not related with the yield. Since the harvest date of crops differs, it was decided to segregate the crops based on harvest dates to get more reliable result.

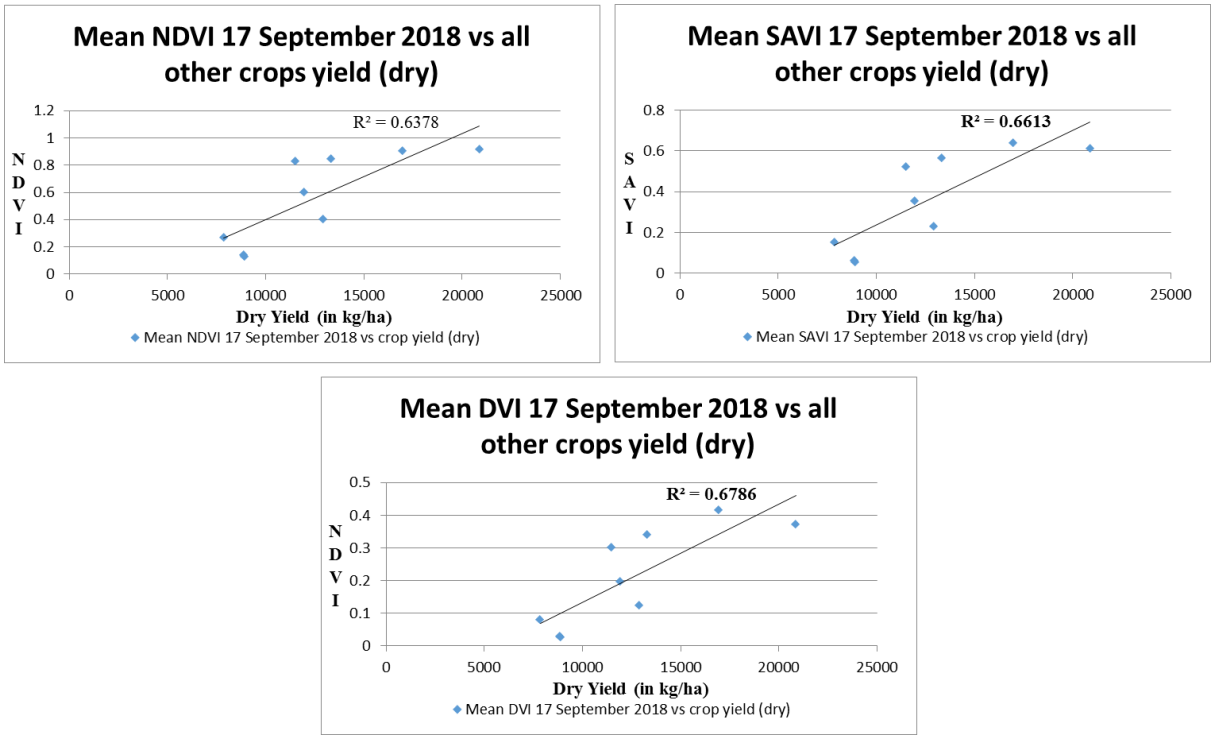

Figure 24: Scatter plot shows relationship between VIs (NDVI, SAVI and DVI) calculated from September 17, 2018 dataset and dry crop yield (other crops), n=9.

The best correlation coefficient for crop yield and VIs of all other crops for 17 September 2018 dataset can be seen in the Figure 23. But the results cannot be considered reliable, as most of the crops were harvested long before that date.

Table 11: Correlation analysis between all other crops yield and corresponding vegetation index (9 plots with 1 plot each for Faba bean/Spring wheat, Winter wheat/Insowed Ley, Spring barley/Lupine, Winter wheat, Sugar beet, Spring barley, Oilseed rape, Kernza and Kernza/lucern.

All other crops except Legume ley (Dry weight)						
NDVI	11th May	13th June	26th July	21st August	04th September	17th September
Pearson	0.18	-0.31	0.30	0.40	0.58	0.80
Spearman	0.27	-0.08	-0.48	0.55	0.67	0.87
SAVI						
Pearson	0.20	-0.19	0.38	0.46	0.59	0.81
Spearman	0.25	-0.08	0.57	0.52	0.62	0.85
DVI						
Pearson	0.19	-0.09	0.49	0.47	0.60	0.82
Spearman	0.25	-0.10	0.48	0.50	0.68	0.85

The relationship of yield and respective VIs of the three crops (Winter wheat/Unsowed Ley, Winter wheat and Oilseed rape) based only on harvest dates exhibited a very strong correlation coefficient with VIs of 11 May 2018. While the VIs of 13 June 2018 exhibited weak positive correlation with the Pearson coefficient and moderate negative correlation with the Spearman coefficient in the case of SAVI and DVI. However, the Pearson and Spearman coefficients exhibited moderately positive correlations with the NDVI (Table 12). The results are considered unreliable because of the restricted sample size.

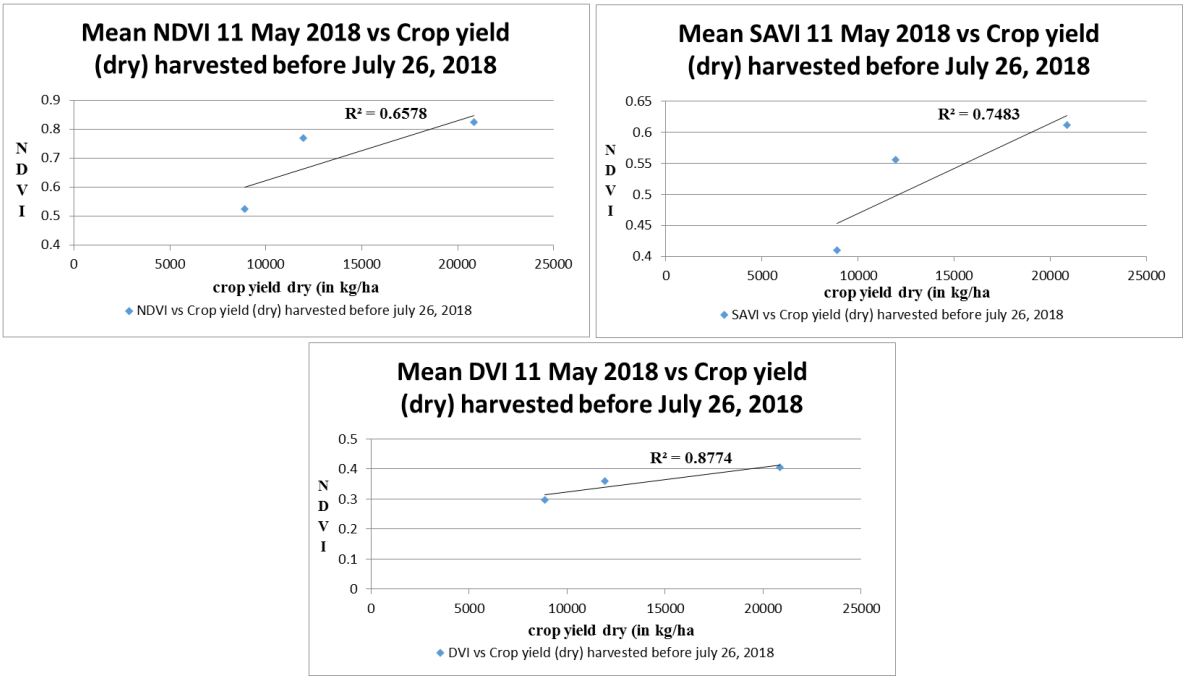

Figure 25: The scatter plots show the relationship between VIs (NDVI, SAVI and DVI) calculated from May 11, 2018 dataset and the dry crop yields (other crops) harvested before July 26, 2018, n=3.

Table 12: Correlation analysis between all other crops yield harvested before 26th July and corresponding VI (3 plots with 1 plot each for Winter wheat/Insowed Ley, Winter wheat, Oilseed rape.

Other crops (except Legume ley) harvested before 26th July		
NDVI	11th May	13th June
Pearson	0.81	0.38
Spearman	1.00	0.50
SAVI		
Pearson	0.87	0.22
Spearman	1.00	-0.50
DVI		
Pearson	0.94	0.12
Spearman	1.00	-0.50

The VIs of crops (Faba bean/Spring wheat, Spring barley/Lupine, Spring barley and Kernza) which were harvested between 26 July 2018 and 21 August 2018, is tabulated in Table 13. On 26 July 2018, NDVI and SAVI showed a moderately strong positive correlation with the crop yield, whereas a weak negative correlation was observed in the case of DVI for both Pearson and Spearman coefficients. On 13 June 2018, all VIs exhibited moderately strong negative relationship with respective crop yields.

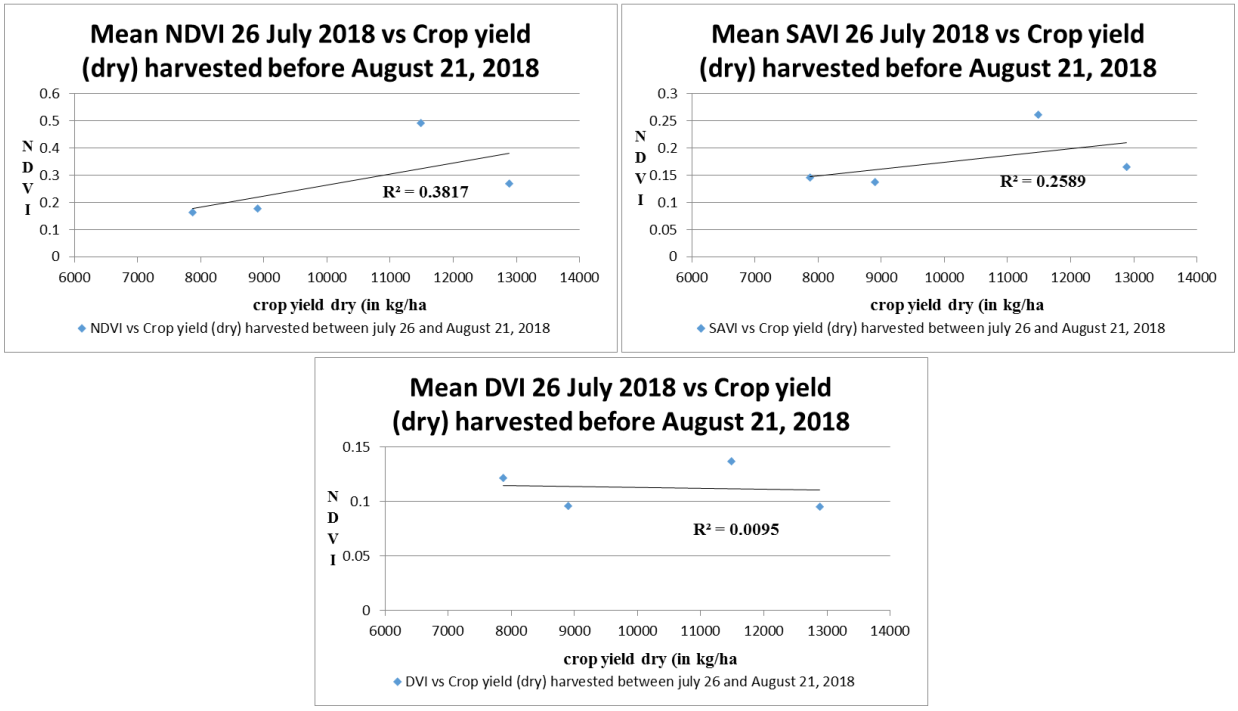

Figure 26: The scatter plots show the relationship between VIs (NDVI, SAVI and DVI) calculated from July 26, 2018 dataset and the dry crop yield (other crops) harvested before August 21, 2018, n=4.

Table 13: Correlation analysis between all other crops yield harvested between 26th July & 21st August and the corresponding VI(3 plots with 1 plot each for Faba bean/Spring wheat, Spring barley/Lupine, Spring barley, Kernza.

Other crops (except Legume ley) harvested between 26th July and 21st August			
NDVI	11th May	13th June	26th July
Pearson	0.18	-0.55	0.62
Spearman	0.00	-0.80	0.80
SAVI			
Pearson	0.18	-0.66	0.51
Spearman	0.00	-0.40	0.60
DVI			
Pearson	0.19	-0.43	-0.10
Spearman	0.00	-0.40	-0.40

6.3. The third research objective was to identify which among the NDVI, SAVI and DVI performed the best to estimate the crop yield. In the case of Legume ley, the best correlation observed was with the Spearman Correlation coefficient (r_s) of 0.89 (for the first harvest) and 0.79 (for the second harvest) for the 'fresh weight' with SAVI. In the case of the other crops, the best correlation for the crops harvested before 26 July 2018 was $r_s = 1$ for all the 3 VIs (with only 3 sample observations); whereas, the crops harvested between 26th July 2018 and 21st August 2018 exhibited the best correlation with $r_s = 0.80$ with NDVI.

Since the relationship between the yield and VIs compared was not linear, it could not be precisely determined which of the VIs are best suited for estimating crop yield. Further experiments are needed to establish the VI that is the best fit for evaluating crop yield.

6.4. The last research objective was to determine if the VIs explain the crop phenology. Although all three VIs exhibited similar trends in crop phenology, they did not reflect the actual crop phenology. Not enough flights data were collected during the growing stages for all the crops. The best crop phenology is explained by the Sugar beet crop (Figure 27).

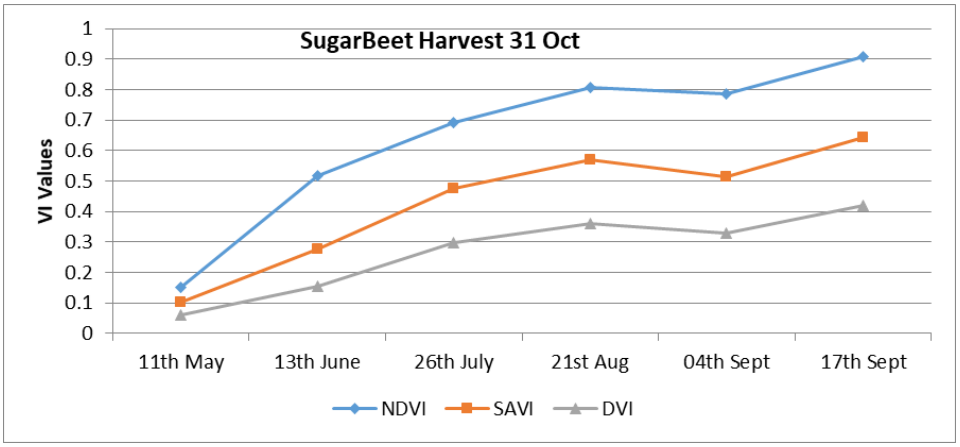

Figure 27: Crop phenology of sugar beet derived from NDVI, SAVI and DVI.

All the plots of the Legume ley exhibited similar phenology irrespective of the management practice employed (conventional or organic). In Figure 28, the Legume Lay phenology with the first harvest on 25 July 2018 is plotted.

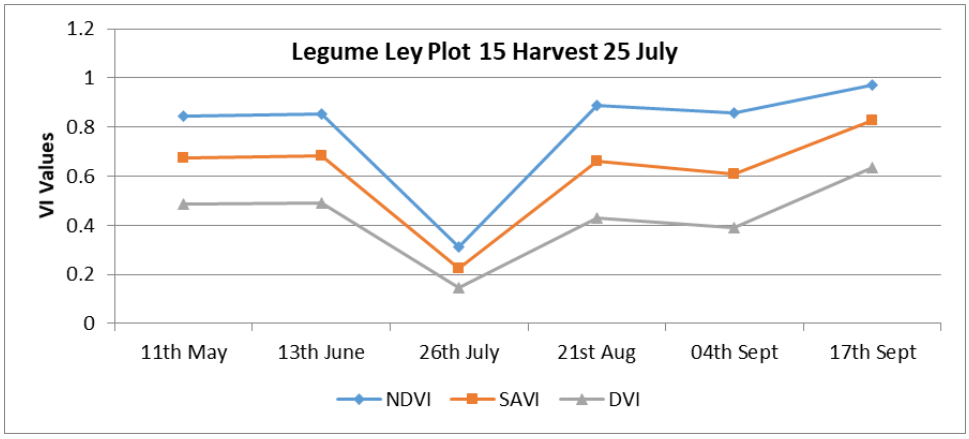

Figure 28: Crop phenology of Legume ley derived from NDVI, SAVI and DVI.

Figure 29 displays the general phenological growth curves for any type of agricultural crop. It should be noted that the phenological pattern may vary with crop species. The plant development from emergence till harvest would generally have a representation of a bell-shaped growth curve; the curve representing the changing VI values. None of the crops in the study area showed this pattern of change in VIs value as a measure of phenology. This is accounted for by the infrequent data capture during various growth phases of the crop. Hence, it is essential to synchronize the frequency of data capture with the major growth stages of the observed crops.

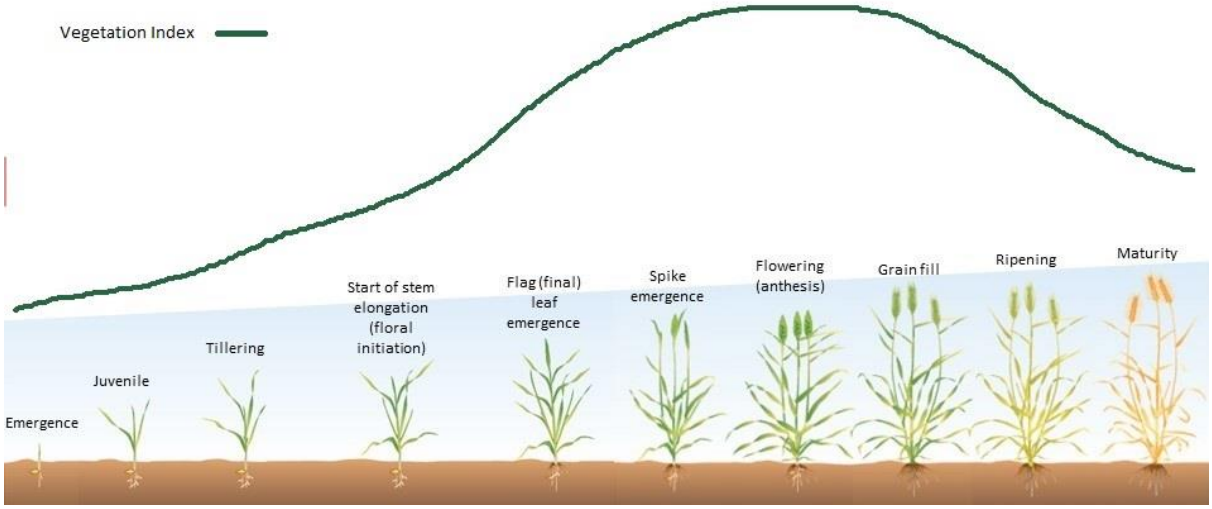

Figure 29: Typical vegetation index curve for plant growth cycle (may differs with crop species). Modified from James Hunt, La Trobe University, AgriBio Centre for Agribiosciences. source;https://grdc.com.au/resources-and-publications/grdc-update-papers/tab-content/grdc-update-papers/2018/08/wheat-phenology-and-the-drivers-for-yield-in-the-high-rainfall-zone

7. Discussion

The Vegetation Index (VI) values observed in the study are relatively high compared to the literature. This could be the result of bias in reflectance values of the reflectance panels due of the angle of the camera or the variations in camera gain due to the fluctuations in the temperature. The study done by (Adler, 2018; Tagle, 2017) found that the NDVI values derived from radiometrically calibrated UAV data tends to have higher values when compared with the NDVI values calculated with that of handheld spectrometer.

All the 3 VIs selected in this study relied on the Red and the NIR bands. Since the NIR band is more sensitive to lower reflectance values than the Red band, it may induce bias if the values in the higher reflectance are saturated. A study by Adler (2018) showed that the Spectralon panel exhibited comparatively high reflectance values than the actual panel reflectance, especially, in the NIR band at higher altitudes (i.e. > 60m) as compared to linear relation at 50% calibration data. This could be one of the reasons for the higher than normal vegetation index values observed in this study. This observation of the researcher is presented as a table in Appendix figure 20.

The summer of 2018 was unusually warm; one of the hottest in the last 100 years and the temperatures were 2 degrees Celsius higher than the previous highest average monthly temperature at many places (Åström, Bjelkmar, & Forsberg, 2019). Especially, the month of July was exceptionally hot in southern part of Sweden. Data from SHMI (Sveriges meteorologiska och hydrologiska institut) shows that the monthly average temperature of June and July of 2018 was 3 degree Celsius warmer than that of May and July of 2019. This atypical warm season lead to drought like conditions. The scarcity of water and sweltering heat could have affected the growth of the crops. The staff of the SLU confirmed that the crops had less than normal size of leaves and plant height. This could be the impact of water scarcity and heat; however, surprisingly even with the smaller leaves and shorter height, the crop yield was normal. It is possible that the crops may have adapted and reduced the size of the leaves to compensate for the amount of sunlight they needed. The shunted height of the crops could be the result of reduced competition for solar energy or due to the scarcity of water. The size of the leaves and the height would affect the vegetation index. This may be one of the factors for low vegetation index values calculated in July and August 2018. Although the warm summer affected all the crops in the study area, the crop specific response to the heat stress would be different. Further research initiatives need to be undertaken to focus on understanding the response of each crop to heat stress to arrive at any conclusion.

Vegetation indices for the dataset captured on 26 July 2018 has comparatively very low values than the other datasets. Even if this dataset had relatively better correlation with yield compared to the correlation with the same variable in other time frames, it was observed

that the images appeared relatively darker (Appendix C Figure C1). However, from the observation of the strong shadows of the trees in the study area, it was discerned that the day was particularly sunny and bright. After the analysis of the EXIF data (i.e. Exchangeable Image File), it was discovered that the automatic settings of the camera increased the shutter speed. It was found to be approximately 10 times quicker than other datasets in all the four bands but especially in case of the RedEdge and the NIR bands. In addition to this, it was also observed that the sensor temperature of the 26 July 2018 dataset was approximately 10 degrees Celsius higher than corresponding datasets captured from the rest of the flights for all available bands (20 degree Celsius in case of Red edge band). Such arbitrary fluctuations of the sensor temperature could affect the DN values. Figure A1 (annex section A) exhibits the regressive relationship between the DN and the reflectance values of the reflectance panels. Adler (2018) also identified this behavior of Sequoia sensor to have introduced consistent noise (result of his experiment showing noise due to temperature increment is shown in annex Figure A2 in all four bands; this effect changes the pixel values as shown in annex Figure A3.

Comparing the result of the VIs from the Sequoia sensor with that of the fixed tower sensor, uniform offset was observed (i.e. the VIs calculated from the fixed tower sensor were consistently lower than the flight sensors). It was previously discussed that the radiometrically calibrated UAV data tends to overestimate the vegetation indices. But, in the case of the fixed tower sensors the sensitivity of sensors is taken as optimum (K-factor = 1) as though is it working as new. The performance of these sensors degrades with time and needs to be adjusted for better performance by changing the k-factor. Limited knowledge of the technology restricted the adjustment of the k-factor; therefore, the study did not make use of the sensitivity factor to explain the offset between the different sensors. The variations in the band width as well as the mean wavelength of the NIR and the Red band for the Sequoia and the tower sensor potentially could have impacted the vegetation indices. The reason for the overestimation in the VI values could also be explained by the fact that the mean NDVI values of the whole plot from UAV sensor is compared with the VI from the small footprint area of the fixed tower sensors.

With regards to the second research question “do vegetation indices explain crop yield?”, the results indicated that the VIs are not great indicators of the crop yield for the crops of interest. However, vegetation indices can be good indicators for the yield; this strongly depends on the type of the crops being monitored. The correlation between VI and crop yield is appropriate and provides satisfactory results when the yield is directly dependent on the leaves (e.g. in the case of grass or leafy crops); it becomes less relevant when the yield depends on the small fruits of plant with many leafs (e.g. in case of Strawberries or potatoes). This is due to VIs being good indicators of the “greenness”, i.e. the intensity of the live vegetation. So, it is concluded that if the VIs of different types of crop is considered with

their corresponding yields holistically as a single relationship, it may result in poor relationship as found in this study.

This raises the question why the relationship between each crop type along with their respective yield was not established. This would have been ideal, however due to the lack of historical crop yield data (i.e. data was available from only one growth cycle in most cases), and since the study was limited to only one replicate of the study area, it was not possible to generate and establish a reliable statistical relationship.

Furthermore, different crops have different lifecycles and have very different reflectance values during the various growth stages. Guan et al. (2019) claimed that there is a relationship between VI and yield, and this relationship changes with phenological growth stage. They observed the strong relationship between NDVI and wheat yield only from the flowering stage till the ripening stage. This implies that not all stages of crop cycle are strongly related to the yield. This is a possible factor for the varying correlation between VIs and yield. The UAV data that would have captured those phenological stages of the crops to establish the relationship between VI at that stage with the corresponding yield was not available. Therefore, it remains inconclusive of how effective VIs could be used for predicting yield.

Additionally, management routine such as application of fertilizers and herbicides can affect the reflectance of the crops. If the images were taken within a few days of fertilizer application, it would alter the reflectance response, since it takes few days for crops to completely absorb the chemicals. As per metadata available, the fertilization and herbicides are applied at different times for different crops and on few occasions, it was administered just a few days before image acquisition (Guan et al., 2019). Consequently, estimating phenological parameters becomes more challenging in the case of intercropping, where it is difficult to differentiate the radiometric characteristics of each species. The plots with multiple crops did not show clear phenology and need to be investigated by crop specific experiments to clearly understand the phenology.

Considering, that the yield of crops is estimated on the basis of extrapolation from the data collected from one small sample patch (0.25 to 1 square meters) for each plot; this could introduce some uncertainties as the crops may have some intra-variability in the fields. Even the small bias could make substantial impact especially when the sample size is small

In addition, the irradiance compensation was not done even though the data from sunshine sensor was available. In an optimal situation we could have used only irradiance data from the sunshine sensor and exposure compensated Sequoia images to get the surface reflectance. This entails having the same units for both the sunshine sensors and exposure

compensated images; and furthermore, that the sunshine sensor gives accurate data. Unfortunately, the alignment of the sunshine sensor (angle/direction with respect to the sun) influences the data in sunny condition (in case of direct light). Additionally, the orientation (roll-pitch-yaw) data from the sunshine sensor's IMU is not accurate; consequently, it was not possible to do the cosine correction with good results. In normal sunny conditions, the irradiance is stable during the short time period of a flight. So, the reflectance panels were used to get reflectance with the empirical line method.

Furthermore, the images were collected for all the plots concurrently irrespective of the different sowing and harvesting dates. The interval between data collection was not uniform and varied throughout the season. Occasionally, the data was collected just after the harvest or long before the harvest resulting in inconsistent phenology.

8. Conclusions

The primary objective of this study was to develop and test a robust methodology for calculating and quantifying vegetation reflectance from a multispectral sensor on a UAV platform. It can be safely concluded that the radiometric correction techniques incorporated in this study gave reasonably good results.

However, the study did not find a strong relationship between the three popular VIs tested (i.e., DVI, NDVI, SVI) and respective crop yields for the various crops of interest in all the cases, Nonetheless strong associations were identified at different growth stages of crops. More research needs to be done to establish a reliable relationship between growth stages and yield of the crop. Therefore, there is not enough evidence to confidently say that vegetation index derived from multispectral UAV images can help estimate crop yield.

Although all three VIs used in this study exhibited the same trend in the phenology, the correlation coefficient with the yield differed on the scale from low to moderate. We also compared the VIs from the UAV sensor with the corresponding VIs from the fixed sensor tower for one plot and found the same phenological trend in the data collected from both the sensors. However, there was a consistent but uniform difference in VIs collected from the UAV and fixed tower sensor. This indicates that there is a systematic error in either one of the sensors.

Furthermore, to validate the reliability of radiometric correction and derived VIs, we compared the VIs of each plot with the crop height of the corresponding plots and found moderately strong positive correlation. Therefore, to conclude, even though there is still certain level of uncertainty involving radiometric calibration, the results of radiometric calibration in this study were good enough to be used for understanding vegetation phenomenon and the yields.

In some cases, moderately positive to strong positive correlation between the VIs and the yield was observed. However, there were few dates when we observed very strong negative correlation. There are many factors which influence the outcomes and this prevents arriving at any conclusion with high confidence.

9. Recommendations

The research revealed that there were many uncertainties in the data. To address this in further studies, we recommend making some modifications to the data collection strategy. Data collected more frequently such as on a fortnightly basis would have captured the finer detail of the phenological changes; this would reflect the various phenological stages. Crops have different life cycle periods; the number of flight should be determined based on the crop type being monitored. Furthermore, flights should be avoided just after the field management practices (such as fertilizers & herbicides application and harvesting). A potential research would study the effect of pre- and post- application of fertilizer on collected data as well as its effects on the reflection behavior of the plants. Another suggestion is to collect the UAV data around noon and to keep the time of data collection uniform over all the flights.

Since only a single sample per plot was collected from a very small area (0.25 square meters – 1 square meter), even a small error in measurement would change result to a great extent when it is extrapolated for the entire plot. It is recommended to take at least three samples per plot and to average the results. The recording of geolocation of sampling points establishes more accurate relationship between different crop parameters. Furthermore, instead of using the mean VI values for the entire plot, it is recommended to divide the plot into 5x5 meter grids to extract the VI values. This would enable capturing the spatial variation of the VIs in a more detailed manner than just depending on single average value of the entire plot.

It is also suggested to use the data from all the replicates (SAFE A, B, C and D) to have sufficient number of samples for relevant comparison and crop specific analysis.

10. References

Adler, K. (2018). Radiometric correction of multispectral images collected by a UAV for phenology studies. (Master of Science (MSc)), Lund University, (Student thesis series INES nr 457)

Agisoft LLC. (2018). *Agisoft PhotoScan User Manual: Professional Edition, Version 1.4*.

Åström, C., Bjelkmar, P., & Forsberg, B. (2019). High mortality during the 2018 heatwave in Sweden. *Lakartidningen, 116*.

Beisl, U., & Woodhouse, N. (2004). Correction of Atmospheric and bidirectional Effects in Multispectral ADS40 Images for Mapping Purposes.

Bendig, J., Yu, K., Aasen, H., Bolten, A., Bennertz, S., Broscheit, J., . . . Bareth, G. (2015). Combining UAV-based plant height from crop surface models, visible, and near infrared vegetation indices for biomass monitoring in barley. *International Journal of Applied Earth Observation and Geoinformation, 39*, 79-87. doi:10.1016/j.jag.2015.02.012

Candiago, S., Remondino, F., De Giglio, M., Dubbini, M., & Gattelli, M. (2015). Evaluating Multispectral Images and Vegetation Indices for Precision Farming Applications from UAV Images. *Remote Sensing, 7*(4), 4026-4047. doi:10.3390/rs70404026

Clark, B., Suomalainen, J., & Pellikka, P. (2011a). An historical empirical line method for the retrieval of surface reflectance factor from multi-temporal SPOT HRV, HRVIR and HRG multispectral satellite imagery. *International Journal of Applied Earth Observation and Geoinformation, 13*(2), 292-307.

Clark, B., Suomalainen, J., & Pellikka, P. (2011b). The selection of appropriate spectrally bright pseudo-invariant ground targets for use in empirical line calibration of SPOT satellite imagery. *ISPRS journal of photogrammetry and remote sensing, 66*(4), 429-445.

Clemens, S. R. (2012). Procedures for correcting Digital Camera Imagery Acquired by the AggieAir remote sensing platform, *All Graduate Plan B and other Reports*. 186. https://digitalcommons.usu.edu/gradreports/186.

Dall'Asta, E., & Roncella, R. (2014). A Comparison of Semiglobal and Local Dense Matching Algorithms for Surface Reconstruction. *International Archives of the Photogrammetry, Remote Sensing & Spatial Information Sciences, 45*.

Daughtry, C. S. T., Walthall, C. L., Kim, M. S., de Colstoun, E. B., & McMurtrey, J. E. (2000). Estimating Corn Leaf Chlorophyll Concentration from Leaf and Canopy Reflectance. *Remote Sensing of Environment, 74*(2), 229-239. doi:https://doi.org/10.1016/S0034-4257(00)00113-9

De Biasio, T. A. M., Fritz, A., & Leitner, R. (2013). UAV-based Measurement of Vegetation Indices for Environmental Monitoring. *2013 Seventh International Conference on Sensing Technology (Icst)*, 704-707.

Di Gennaro, S. F., Rizza, F., Badeck, F. W., Berton, A., Delbono, S., Gioli, B., . . . Matese, A. (2018). UAV-based high-throughput phenotyping to discriminate barley vigour with visible and near-infrared vegetation indices. *International Journal of Remote Sensing, 39*(15-16), 5330-5344. doi:10.1080/01431161.2017.1395974

DroneDeploy. (2017). Choosing the Right Mapping Drone for Your Business Part I: Multi-Rotor vs. Fixed Wing Aircraft. Retrieved from https://blog.dronedeploy.com/choosing-the-right-mapping-drone-for-your-business-part-i-multi-rotor-vs-fixed-wing-aircraft-6ec2d02eff48

Dunford, C. (2009). Credit unions and rural banks reaching down and out to the rural poor through group-based microfinance. *Enterprise Development and Microfinance, 20*(2), 107-124.

Effiom, A. E. (2018). UAV-RGB and Multispectral Pleiades images for tree species identification and forest carbon estimation in Amtsvenn, Germany. (Master of Science (MSc)), University of Twente,

Fan, M., Shen, J., Yuan, L., Jiang, R., Chen, X., Davies, W. J., & Zhang, F. (2011). Improving crop productivity and resource use efficiency to ensure food security and environmental quality in China. *Journal of experimental botany, 63*(1), 13-24.

FAO. (2009). High Level Expert Forum - How to Feed the World in 2050. Retrieved from http://www.fao.org/fileadmin/templates/wsfs/docs/Issues_papers/HLEF2050_Global_Agriculture.pdf

Georgiev, G. T., & Butler, J. J. (2007). Long-term calibration monitoring of Spectralon diffusers BRDF in the air-ultraviolet. *Applied Optics, 46*(32), 7892-7899.

Gitelson, A. A. (2004). Wide Dynamic Range Vegetation Index for Remote Quantification of Biophysical Characteristics of Vegetation. *Journal of Plant Physiology, 161*(2), 165-173. doi:https://doi.org/10.1078/0176-1617-01176

Gómez-Candón, D., De Castro, A., & López-Granados, F. (2014). Assessing the accuracy of mosaics from unmanned aerial vehicle (UAV) imagery for precision agriculture purposes in wheat. *Precision Agriculture, 15*(1), 44-56.

GSARS. (2017). Methodology for Estimation of Crop Area and Crop Yield under Mixed and Continuous Cropping. Retrieved from http://gsars.org/wp-content/uploads/2017/03/TR-15.03.2017-Methodology-for-Estimation-of-Crop-Area-and-Crop-Yield-under-Mixed-and-Continuous-Cropping.pdf

Guan, S., Fukami, K., Matsunaka, H., Okami, M., Tanaka, R., Nakano, H., . . . Takahashi, K. (2019). Assessing Correlation of High-Resolution NDVI with Fertilizer Application Level and Yield of Rice and Wheat Crops using Small UAVs. *Remote Sensing, 11*(2), 112.

Guo, Y., Senthilnath, J., Wu, W., Zhang, X., Zeng, Z., & Huang, H. (2019). Radiometric calibration for multispectral camera of different imaging conditions mounted on a UAV platform. *Sustainability, 11*(4), 978.

Hinkle, D. E., Wiersma, W., & Jurs, S. G. (2003). *Applied statistics for the behavioral sciences* (Vol. 663): Houghton Mifflin College Division.

Huete, A. R. (1988). A soil-adjusted vegetation index (SAVI). *Remote sensing of environment, 25*(3), 295-309.

Hunt, E. R., Cavigelli, M., Daughtry, C. S. T., McMurtrey, J. E., & Walthall, C. L. (2005). Evaluation of Digital Photography from Model Aircraft for Remote Sensing of Crop Biomass and Nitrogen Status. *Precision Agriculture, 6*(4), 359-378. doi:10.1007/s11119-005-2324-5

Japan Association of Remote Sensing. (1999). Chapter 9 Image Processing - Correction. Retrieved from http://wtlab.iis.u-tokyo.ac.jp/wataru/lecture/rsgis/rsnote/cp9/cp9-1.htm

Jin, H. X., & Eklundh, L. (2015). In Situ Calibration of Light Sensors for Long-Term Monitoring of Vegetation. *IEEE Transactions on Geoscience and Remote Sensing, 53*(6), 3405-3416. doi:10.1109/Tgrs.2014.2375381

Laboratory, C. V. (2019). Image-Based Plant Phenotyping. Retrieved from https://www.nottingham.ac.uk/research/groups/cvl/projects/plant-phenotyping/plant-phenotyping.aspx

Maine, W. (2018). *Practical Use of Drones to Address Management Problems in Coastal Zones*. Retrieved from http://www.act-us.info/Download/Workshops/2018/Drone.pdf

Mitchell, H. B. (2010). Image fusion: theories, techniques and applications, *Springer Science & Business Media*.

Mróz, M., & Sobieraj-Żłobińska, A. (2004). Comparison of several vegetation indices calculated on the basis of a seasonal SPOT XS time series, and their suitability for land cover and agricultural crop identification. *Tech. Sci., 7*, 39-66.
Mukaka, M. M. (2012). A guide to appropriate use of correlation coefficient in medical research. *Malawi Medical Journal, 24*(3), 69-71.
Parrot Sequoia. (2017). *Parrot Sequoia User Guide*.
Pettorelli, N. (2013). The normalized difference vegetation index, *Oxford University Press*.
Pinzon, J., & Tucker, C. (2014). A non-stationary 1981–2012 AVHRR NDVI3g time series. *Remote Sensing, 6*(8), 6929-6960.
Possoch, M., Bieker, S., Hoffmeister, D., Bolten, A., Schellberg, J., & Bareth, G. (2016). Ulti-Temporal Crop Surface Models Combined with the Rgb Vegetation Index from Uav-Based Images for Forage Monitoring in Grassland. *Xxiii Isprs Congress, Commission I, 41*(B1), 991-998. doi:10.5194/isprsarchives-XLI-B1-991-2016
Rouse Jr, J. W., Haas, R., Schell, J., & Deering, D. (1974). Monitoring vegetation systems in the Great Plains with ERTS.
SARE. (2019). Correlating Nitrogen Application Rates in Sugarcane With Low-Cost Normalized Difference Vegetation Index (NDVI). Retrieved from https://projects.sare.org/sare_project/fs14-282/
Senthilnath, J., Kandukuri, M., Dokania, A., & Ramesh, K. N. (2017). Application of UAV imaging platform for vegetation analysis based on spectral-spatial methods. *Computers and Electronics in Agriculture, 140*, 8-24. doi:10.1016/j.compag.2017.05.027
Singh, R. (n.d.). Crop Yield Estimation and Forecasting Using Remote Sensing. In.
Smith, G. M., & Milton, E. J. (1999). The use of the empirical line method to calibrate remotely sensed data to reflectance. *International Journal of remote sensing, 20*(13), 2653-2662.
Tagle, X. (2017). Study of radiometric variations in Unmanned Aerial Vehicle remote sensing imagery for vegetation mapping. (Master of Science (MSc)), Lund University

University of Twente, (Lund University GEM thesis series nr 23)
Tucker, C. J. (1979). Red and photographic infrared linear combinations for monitoring vegetation. *Remote sensing of Environment, 8*(2), 127-150.
Tucker, C. J., Pinzon, J. E., Brown, M. E., Slayback, D. A., Pak, E. W., Mahoney, R., . . . El Saleous, N. (2005). An extended AVHRR 8-km NDVI dataset compatible with MODIS and SPOT vegetation NDVI data. *International Journal of Remote Sensing, 26*(20), 4485-4498.
Vega, F. A., Ramírez, F. C., Saiz, M. P., & Rosúa, F. O. (2015). Multi-temporal imaging using an unmanned aerial vehicle for monitoring a sunflower crop. *Biosystems Engineering, 132*, 19-27. doi:10.1016/j.biosystemseng.2015.01.008
Wang, C., & Myint, S. W. (2015). A simplified empirical line method of radiometric calibration for small unmanned aircraft systems-based remote sensing. *IEEE Journal of Selected Topics in Applied Earth Observations and Remote Sensing, 8*(5), 1876-1885.
Wijesingha, J. (2016). Geometric quality assessment of multi-rotor unmanned aerial vehicle borne remote sensing products for precision agriculture. (Master of Science (MSc)), Lund University, (Student thesis series INES nr 401)
Yemane Tumlisan, G. (2017). *Monitoring Growth Development and Yield Estimation of Maize Using Very High-Resolution UAV Images in Gronau, Germany*. (Master of Science (MSc)), University of Twente,

Yu, N., Li, L., Schmitz, N., Tian, L. F., Greenberg, J. A., & Diers, B. W. (2016). Development of methods to improve soybean yield estimation and predict plant maturity with an unmanned aerial vehicle based platform. *Remote Sensing of Environment, 187*, 91-101. doi:10.1016/j.rse.2016.10.005

Yue, J., Yang, G., Li, C., Li, Z., Wang, Y., Feng, H., & Xu, B. (2017). Estimation of Winter Wheat Above-Ground Biomass Using Unmanned Aerial Vehicle-Based Snapshot Hyperspectral Sensor and Crop Height Improved Models. *Remote Sensing, 9*(7). doi:10.3390/rs9070708

Zhang, C., & Kovacs, J. M. (2012). The application of small unmanned aerial systems for precision agriculture: a review. *Precision agriculture, 13*(6), 693-712.

Zhou, X., Zheng, H. B., Xu, X. Q., He, J. Y., Ge, X. K., Yao, X., . . . Tian, Y. C. (2017). Predicting grain yield in rice using multi-temporal vegetation indices from UAV-based multispectral and digital imagery. *Isprs Journal of Photogrammetry and Remote Sensing, 130*, 246-255. doi:10.1016/j.isprsjprs.2017.05.003

Ziliani, M., Parkes, S., Hoteit, I., & McCabe, M. (2018). Intra-Season Crop Height Variability at Commercial Farm Scales Using a Fixed-Wing UAV. *Remote Sensing, 10*(12). doi:10.3390/rs10122007

11. Appendix

Appendix A

Sequoia temperature vs image mean pixel value

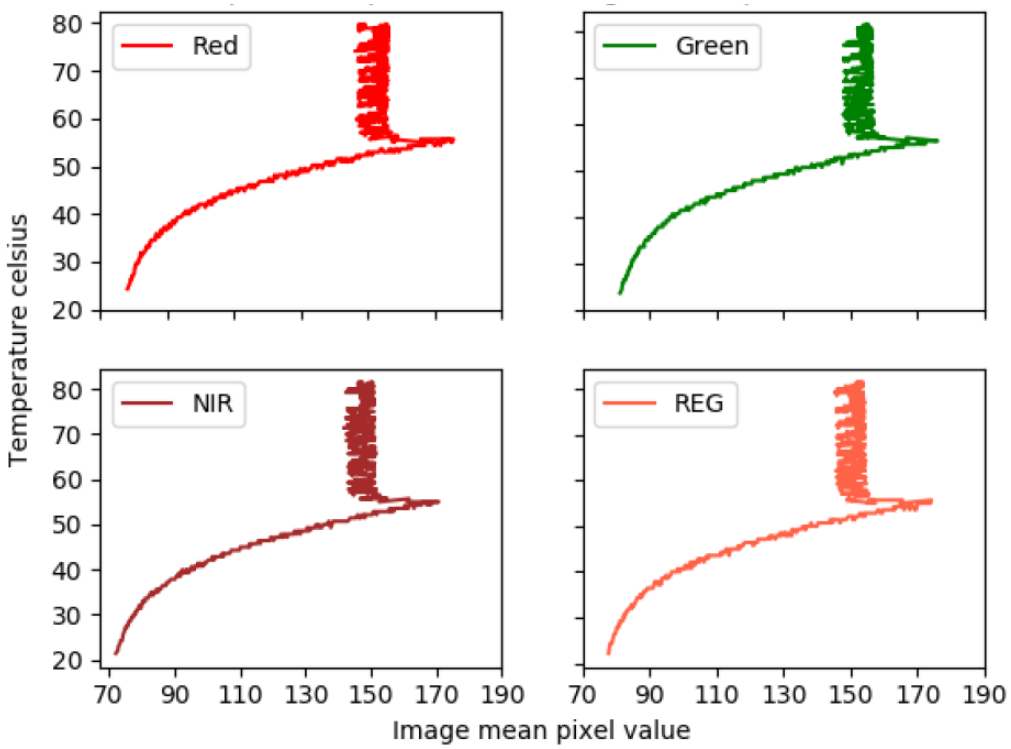

Figure A1: Sequoia Mean pixel value response to temperature (Adler, 2018), The plot shows the temperature versus the image mean pixel value for the Parrot Sequoias four individual camera sensors for a 35-minute dark current test with automatic camera setting. The x axis represents the image mean pixel value i.e. the mean value for the whole image. The y-axis represents the temperature in Celsius. Recordings were done at a 1.5 second interval.

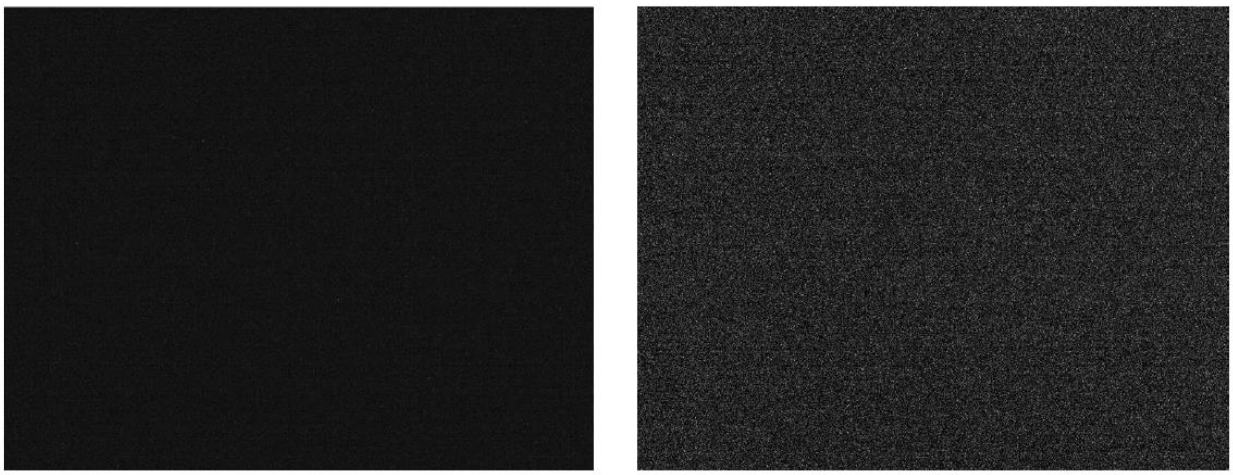

Figure A230: Dark current noise for green band in Parrot Sequoia (Adler, 2018), It shows first and the last image taken during the dark current test for the green band in the parrot sequoia camera. To the left is the first image taken and to the right is the last (1397$^{th)}$ image.

*Table following table shows the mean reflectance for each plate present in the field images for the different calibration data and capture height. Reflectance is expressed in decimal form where each plate has a target reflectance acquired from the manufacturer data from each spectralon reflectance panel i.e. column 2 corresponds to the calibration data acquired with the 50% reflectance is derived from assuming the spectral sensitivity within the band in uniform. * = error compared to the target in %. The calculated error is rounded to the closest integer.*

	Reflectance plate	Predicted mean reflectance, 50% calibration at 10 meters	Predicted mean reflectance, 50% calibration at 60 meters	Actual plate reflectance
Green	5%	0.052 *(40%)**	0.052 *(40%)**	0.037
	20%	0.225 *(6%)**	0.203 *(4%)**	0.212
	50%	0.275 *(44%)**	0.273 *(45%)**	0.499
	99%	0.295 *(70%)**	0.279 *(71%)**	0.99
Red	5%	0.042 *(7%)**	0.045 *(15%)**	0.039
	20%	0.202 *(9%)**	0.177 *(20%)**	0.224
	50%	0.288 *(44%)**	0.278 *(46%)**	0.516
	99%	0.293 *(70%)**	0.282 *(71%)**	0.99
NIR	5%	0.07 *(70%)**	0.105 *(150%)**	0.041
	20%	0.234 *(1%)**	0.437 *(83%)**	0.238
	50%	0.508 *(5%)**	0.682 *(27%)**	0.535
	99%	0.755 *(23%)**	0.688 *(30%)**	0.99
REG	5%	0.054 *(35%)**	0.059 *(47%)**	0.04
	20%	0.221 *(5%)**	0.228 *(2%)**	0.232
	50%	0.511 *(3%)**	0.495 *(6%)**	0.528
	99%	0.777 *(22%)**	0.766 *(23%)**	0.99

Figure A3: Predicted mean reflectance at 50% calibration for reflectance panels (Adler, 2018)

Appendix B

Following charts shows the linear relationship between reflectance of spectralon panels and DN values from image datasets.

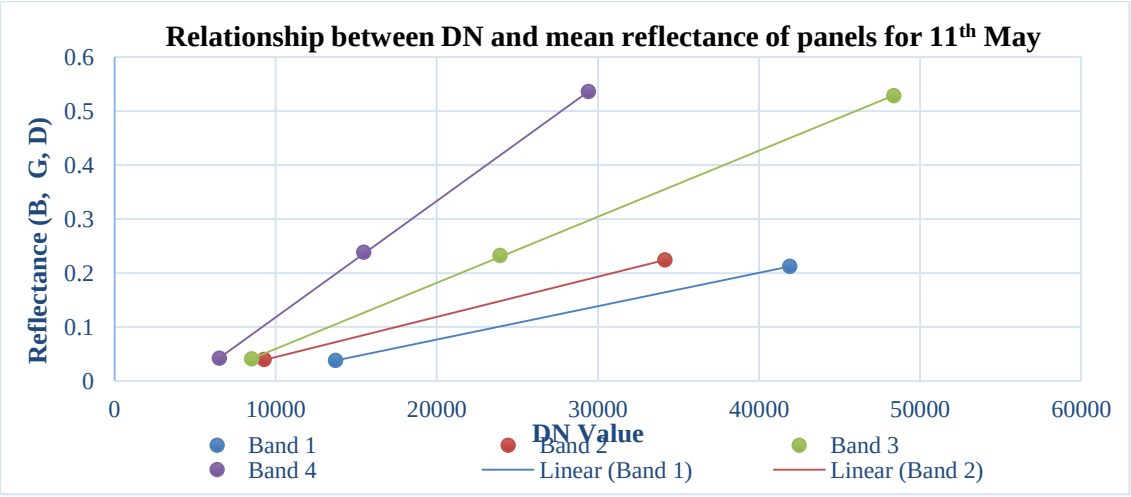

Figure B1: Relationship between DN and mean reflectance of panels for 11th May

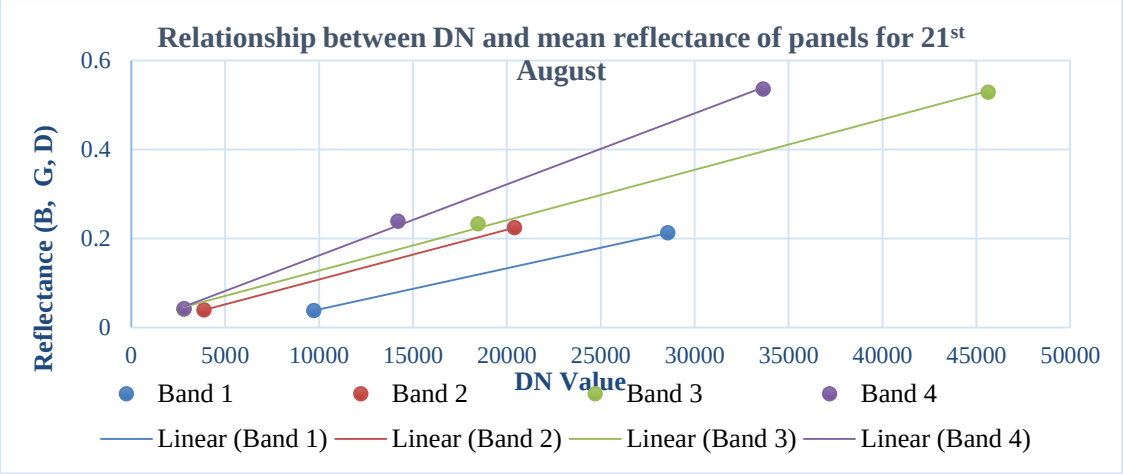

Figure B231: Relationship between DN and mean reflectance of panels for 21st August

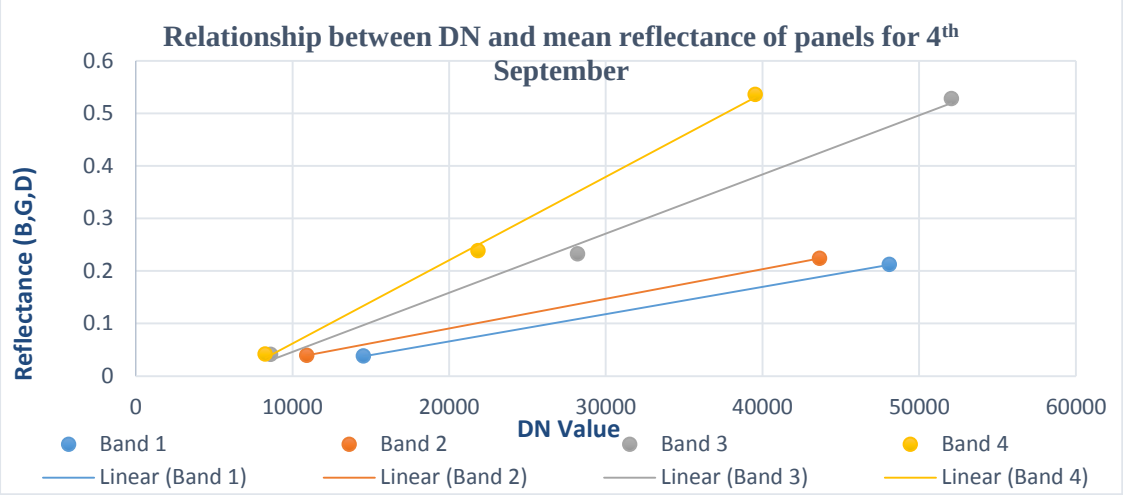

Figure B3: Relationship between DN and mean reflectance of panels for 4th September

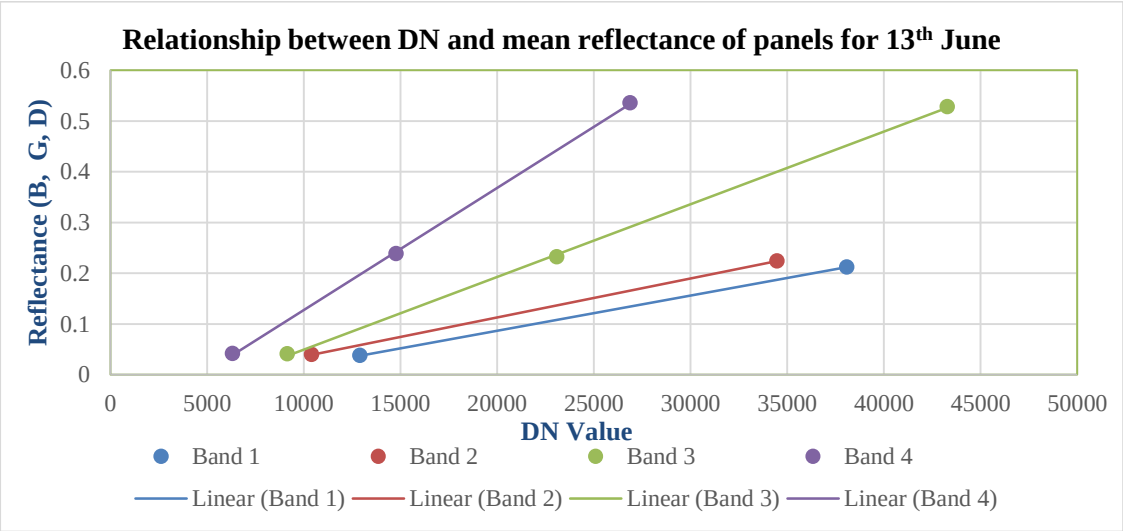

Figure B4: Relationship between DN and mean reflectance of panels for 13th June

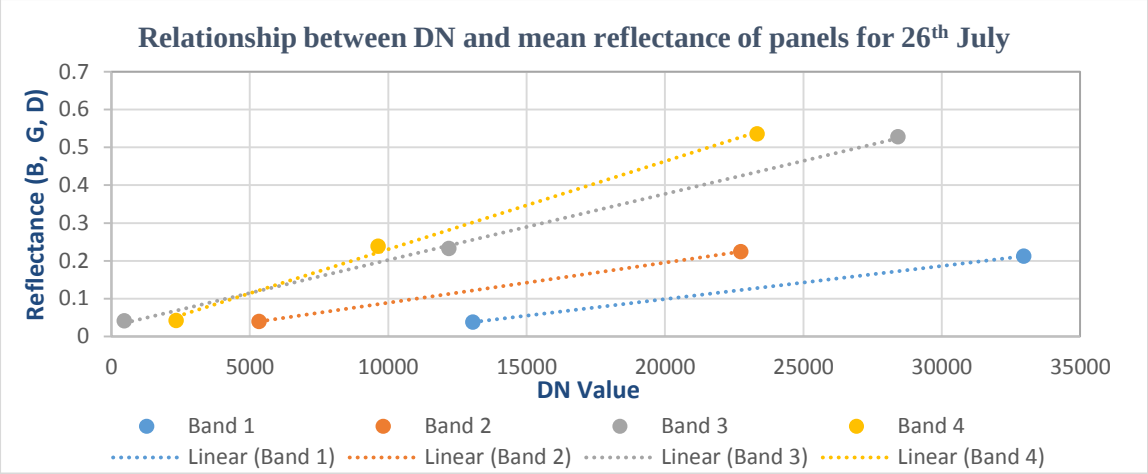

Figure B5: Relationship between DN and mean reflectance of panels for 26th July

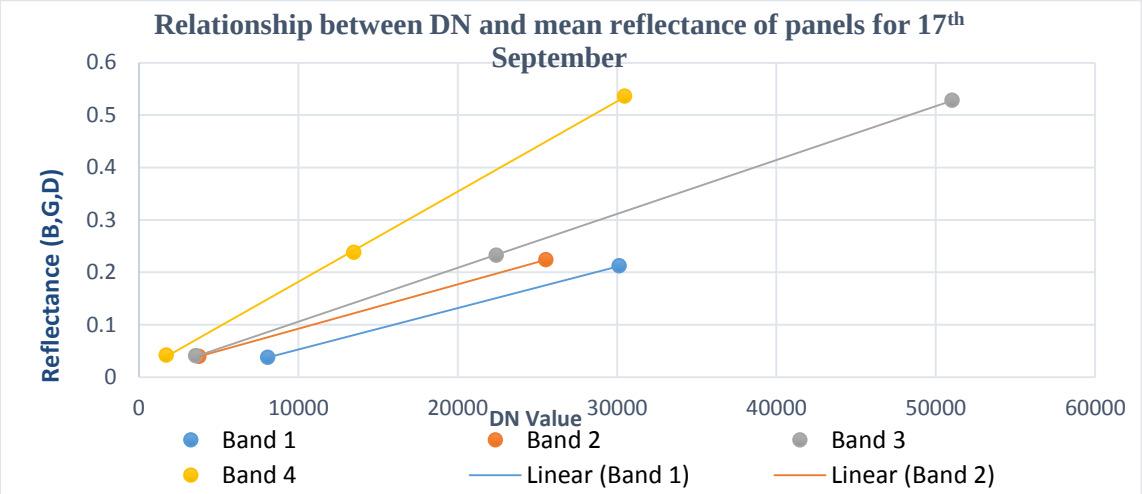

Figure B632: Relationship between DN and mean reflectance of panels for 17th September

Appendix C

Orthomosaics in false colour composite derived from six different datasets gathered from UAV platform over a growing season. (Date of data collection in written below the images (a-f).

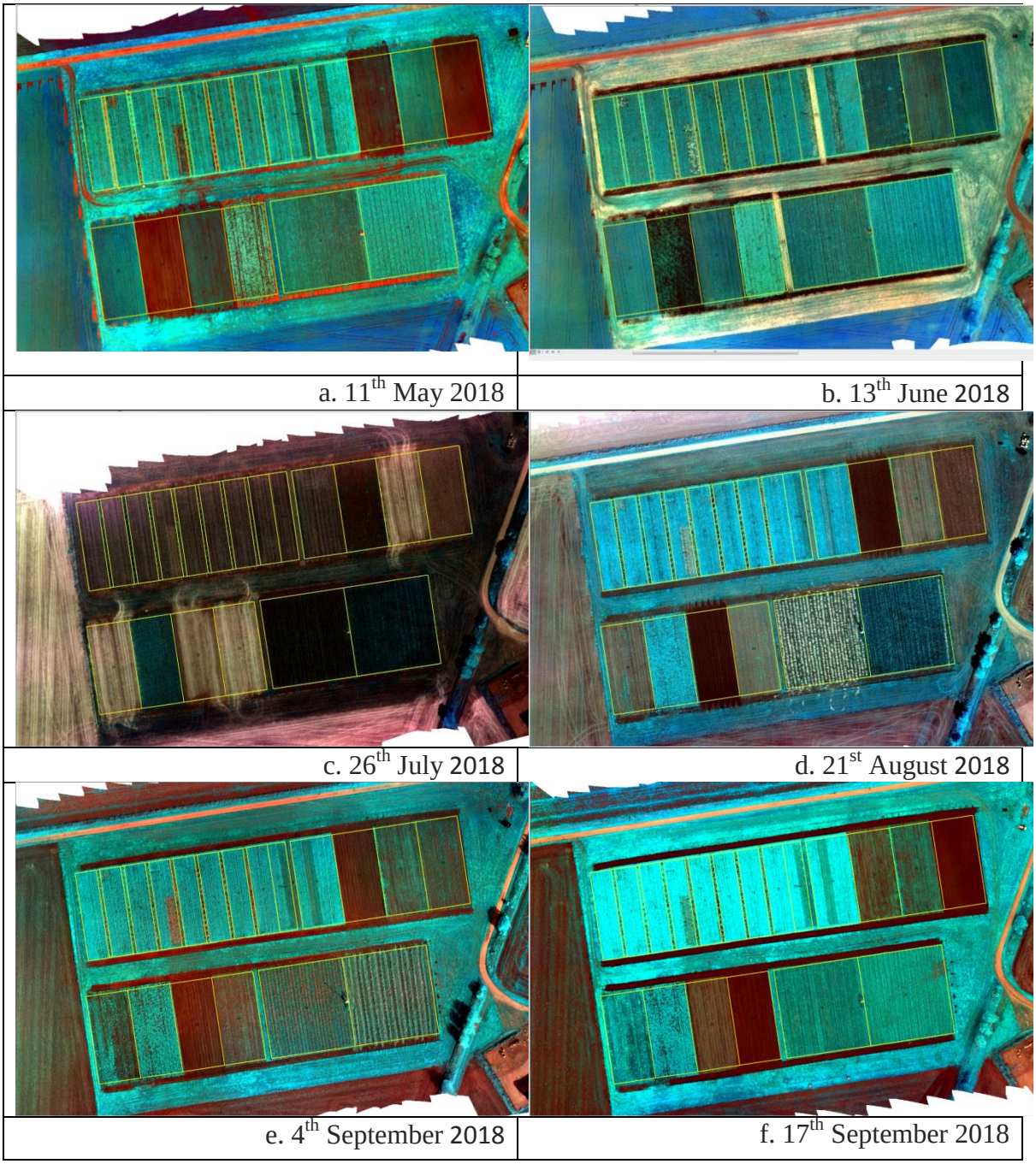

a. 11th May 2018 | b. 13th June 2018

c. 26th July 2018 | d. 21st August 2018

e. 4th September 2018 | f. 17th September 2018

Figure C1: Orthomosaic of 6 UAV flights in false colour composite, Red (band 1), RedEdge(band 2), NIR (band 3).

Appendix D

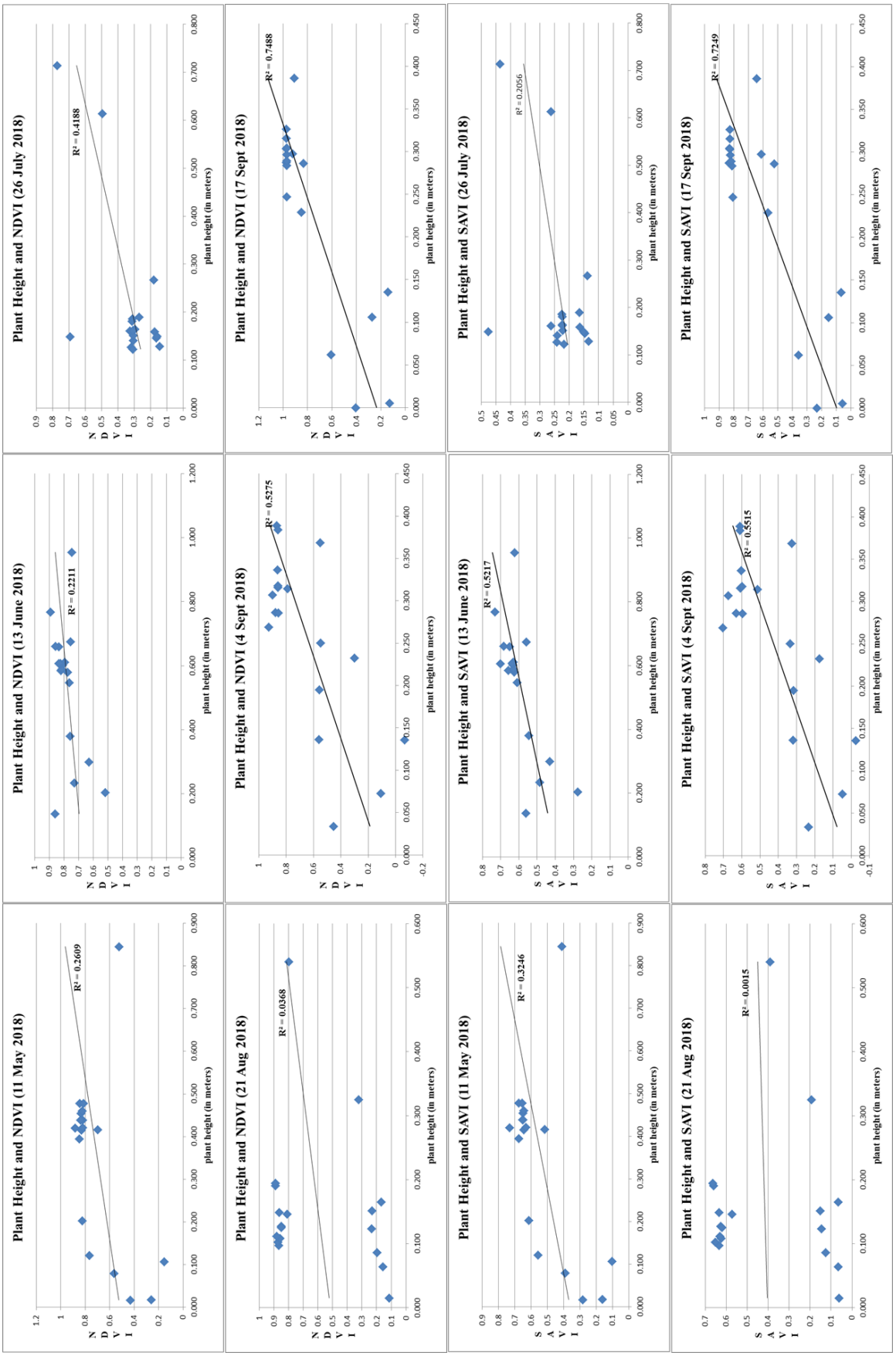

Figure D1and D2: Relationship between plant heights with respective NDVI and SAVI (all 6 datasets)

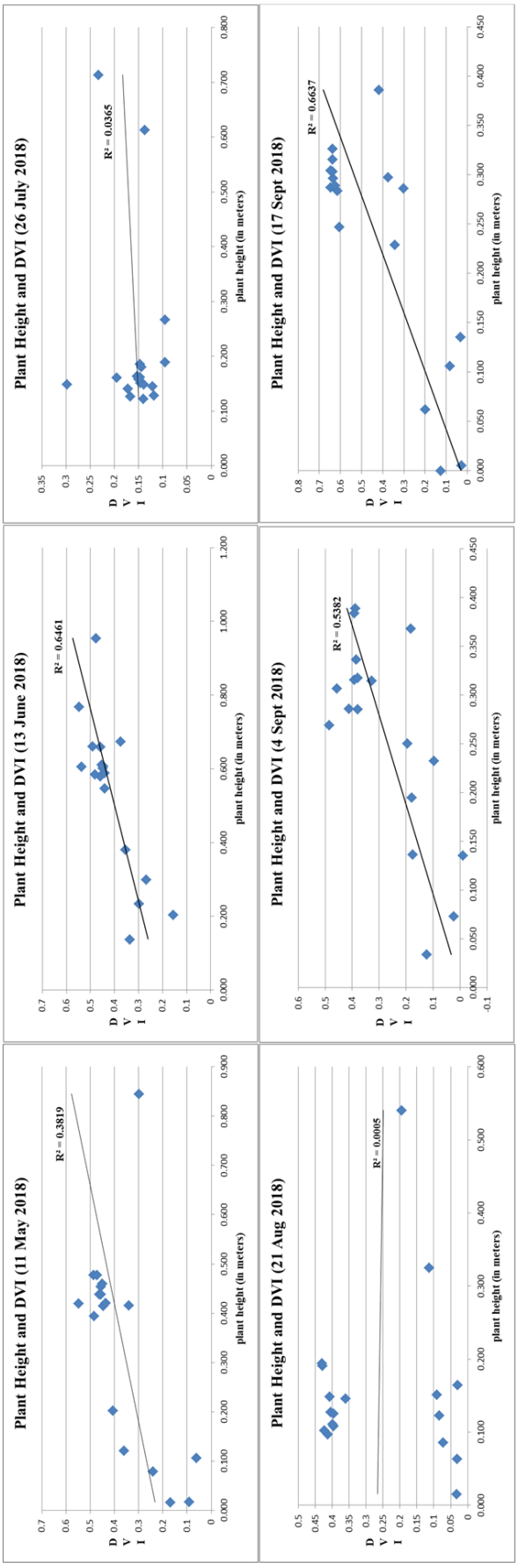

Figure D3: Relationship between plant heights with respective DVI (all 6 datasets)

Department of Physical Geography and Ecosystem Science, Lund University

Lund University GEM thesis series are master theses written by students of the international master program on Geo-information Science and Earth Observation for Environmental Modelling and Management (GEM). The program is a cooperation of EU universities in Iceland, the Netherlands, Poland, Sweden and UK, as well a partner university in Australia. In this series only master thesis are included of students that performed their project at Lund University. Other theses of this program are available from the ITC, the Netherlands (www.gem-msc.org or www.itc.nl).

The student thesis reports are available at the Geo-Library, Department of Physical Geography and Ecosystem Science, University of Lund, Sölvegatan 12, S-223 62 Lund, Sweden. Report series started 2013. The complete list and electronic versions are also electronic available at the LUP student papers (https://lup.lub.lu.se/student-papers/search/) and through the Geo-library (www.geobib.lu.se).

1 Soheila Youneszadeh Jalili (2013) The effect of land use on land surface temperature in the Netherlands

2 Oskar Löfgren (2013) Using Worldview-2 satellite imagery to detect indicators of high species diversity in grasslands

3 Yang Zhou (2013) Inter-annual memory effects between Soil Moisture and NDVI in the Sahel

4 Efren Lopez Blanco (2014) Assessing the potential of embedding vegetation dynamics into a fire behaviour model: LPJ-GUESS-FARSITE

5 Anna Movsisyan (2014) Climate change impact on water and temperature conditions of forest soils: A case study related to the Swedish forestry sector

6 Liliana Carolina Castillo Villamor (2015) Technical assessment of GeoSUR and comparison with INSPIRE experience in the context of an environmental vulnerability analysis using GeoSUR data

7 Hossein Maazallahi (2015) Switching to the "Golden Age of Natural Gas" with a Focus on Shale Gas Exploitation: A Possible Bridge to Mitigate Climate Change?

8 Mohan Dev Joshi (2015) Impacts of Climate Change on *Abies spectabilis*: An approach integrating Maxent Model (MAXent) and Dynamic Vegetation Model (LPJ-GUESS)

9 Altaaf Mechiche-Alami (2015) Modelling future wheat yields in Spain with LPJ-GUESS and assessing the impacts of earlier planting dates

10 Koffi Unwana Saturday (2015) Petroleum activities, wetland utilization and livelihood changes in Southern Akwa Ibom State, Nigeria: 2003-2015

11 José Ignacio Díaz González (2016) Multi-objective optimisation algorithms for GIS-based multi-criteria decision analysis: an application for evacuation planning

12 Gunjan Sharma (2016) Land surface phenology as an indicator of performance of conservation policies like Natura2000

13 Chao Yang (2016) A Comparison of Four Methods of Diseases Mapping

14 Xinyi Dai (2016) Dam site selection using an integrated method of AHP and GIS for decision making support in Bortala, Northwest China

15 Jialong Duanmu (2016) A multi-scale based method for estimating coniferous forest aboveground biomass using low density airborne LiDAR data

16 Tanyaradzwa J. N. Muswera (2016) Modelling maize (Zea Mays L.) phenology using seasonal climate forecasts

17 Maria Angela Dissegna (2016) Improvement of the GPP estimations for Sudan using the evaporative fraction as water stress factor

18 Miguel G. Castro Gómez (2017) Joint use of Sentinel-1 and Sentinel-2 for land cover classification: A machine learning approach

19 Krishna Lamsal (2017) Identifying potential critical transitions in a forest ecosystem using satellite data

20 Maimoona Zehra Jawaid (2017) Glacial lake flood hazard assessment and modelling: a GIS perspective

21 Tracy Zaarour (2017) Application of GALDIT index in the Mediterranean region to assess vulnerability to sea water intrusion

22 Stephania Zabala (2017) Comparison of multi-temporal and multispectral Sentinel-2 and UAV (unmanned aerial vehicle) imagery for crop type mapping

23 Ximena Tagle (2017) Radiometric calibration of unmanned aerial vehicle remote sensing imagery for vegetation mapping

24 Tesfaye Gebeyehu Admasu (2017) Monitoring trends of greenness and LULC (land use/land cover) in Addis Ababa and its surrounding using MODIS time-series and LANDSAT data

25 Haiqi Xu (2017) Development of a digitalization tool for linking thematic data to a background map

26 Zeyao Zhang (2018) BIM to GIS-based building model conversion in support of urban energy simulation

27 Aiman Shahpurwala (2019) Conflict, narratives, and forest fires in eastern Turkey : a quantitative perspective with remote sensing and GIS

28 Ashish Vivekar (2020) Evaluation of methodology for estimating crop yield from multispectral UAV images : a case study at Lönnstorp, Sweden